UC San Diego
UC San Diego Previously Published Works

Title

A multi-dimensional search for new heavy resonances decaying to boosted WW , WZ , or ZZ boson pairs in the dijet final state at 13 Te

Permalink

Journal

European Physical Journal C, 80(3)

Authors

Sirunyan, AM
Tumasyan, A
Adam, W
et al.

Publication Date

2020-03-01

Peer reviewed

THE EUROPEAN
PHYSICAL JOURNAL C

A multi-dimensional search for new heavy resonances decaying to boosted WW, WZ, or ZZ boson pairs in the dijet final state at 13 TeV

CMS Collaboration*

CERN, 1211 Geneva 23, Switzerland

Abstract A search in an all-jet final state for new massive resonances decaying to WW, WZ, or ZZ boson pairs using a novel analysis method is presented. The analysis is performed on data corresponding to an integrated luminosity of 77.3 fb^{-1} recorded with the CMS experiment at the LHC at a centre-of-mass energy of 13 TeV. The search is focussed on potential narrow-width resonances with masses above 1.2 TeV, where the decay products of each W or Z boson are expected to be collimated into a single, large-radius jet. The signal is extracted using a three-dimensional maximum likelihood fit of the two jet masses and the dijet invariant mass, yielding an improvement in sensitivity of up to 30% relative to previous search methods. No excess is observed above the estimated standard model background. In a heavy vector triplet model, spin-1 Z$'$ and W$'$ resonances with masses below 3.5 and 3.8 TeV, respectively, are excluded at 95% confidence level. In a bulk graviton model, upper limits on cross sections are set between 27 and 0.2 fb for resonance masses between 1.2 and 5.2 TeV, respectively. The limits presented in this paper are the best to date in the dijet final state.

1 Introduction

The standard model (SM) of particle physics has been exceptionally successful in accommodating a multitude of experimental measurements and observations, yet it falls short in a variety of aspects. These shortcomings motivate theoretical extensions of the SM that typically introduce new particles, which could be created in proton–proton (pp) collisions at the CERN LHC. In this analysis, we test theoretical models that predict new heavy resonances that decay to pairs of vector bosons (W and Z bosons, collectively referred to as V bosons). These models usually aim to clarify open ques-

tions in the SM such as the large difference between the electroweak and the Planck scales. We consider the bulk scenario of the Randall–Sundrum (RS) model with warped extra dimensions [1–5], where the spin-2 bulk graviton has an enhanced branching fraction to massive particles, and the heavy vector triplet (HVT) framework [6], which serves as a template that reproduces a large class of explicit models predicting spin-1 resonances.

No significant deviations from the SM background expectation have been observed in previous searches by the CMS Collaboration for such particles in the VV [7–11] and VH [12–17] channels, where H denotes the Higgs boson. Similar results were obtained independently by the ATLAS Collaboration in VV [18–21,23,25] and VH [22,24,26] resonance searches. In addition, statistical combinations of diboson and leptonic decay channels of the 2016 data set [27,28] have been performed, which extend the exclusion regions of the individual analyses. Lower limits on the masses of these resonances have been set at the TeV scale. The search presented here focusses on resonances with masses above 1.2 TeV, in the decays of which the vector bosons are produced at high Lorentz boost. Because of the large boost of the vector bosons, their decay products are merged into single, large-radius jets, leading to dijet final states. These jets are identified through dedicated jet substructure algorithms. Compared to previous analyses in this final state [7,10,21–23,29], an improved background estimation and signal extraction procedure based on a three-dimensional (3D) maximum likelihood fit is employed, increasing the sensitivity of the analysis. The method can be applied to any search with final states expected to cause resonant behaviour in three observables, whereas previous methods used solely the invariant mass of the final decay products as the search variable. The improved sensitivity and scope has motivated a reanalysis of the pp collision data collected by the CMS experiment during the 2016 data taking period, as well as a first analysis of the 2017 data set, corresponding to a total

*e-mail: cms-publication-committee-chair@cern.ch

integrated luminosity of 77.3 fb^{-1} at a centre-of-mass energy of 13 TeV.

2 The CMS detector

The central feature of the CMS apparatus is a superconducting solenoid of 6 m internal diameter, providing a magnetic field of 3.8 T. Within the solenoid volume are a silicon pixel and strip tracker, a lead tungstate crystal electromagnetic calorimeter, and a brass and scintillator hadron calorimeter, each composed of a barrel and two endcap sections. Forward calorimeters extend the pseudorapidity (η) coverage provided by the barrel and endcap detectors. Muons are detected in gas-ionization chambers embedded in the steel flux-return yoke outside the solenoid. A more detailed description of the CMS detector, together with a definition of the coordinate system used and the relevant kinematic variables, can be found in Ref. [30].

Events of interest are selected using a two-tiered trigger system [31]. The first level, composed of custom hardware processors, uses information from the calorimeters and muon detectors to select events at a rate of around 100 kHz within a time interval of less than 4 μs. The second level, known as the high-level trigger, consists of a farm of processors running a version of the full event reconstruction software optimized for fast processing, and reduces the event rate to around 1 kHz before data storage.

3 Simulated events

The resonances associated with the considered phenomenologies are the bulk gravitons (G$_{bulk}$) generated for the bulk scenario [3–5] of the RS model of warped extra dimensions [1,2], and the heavy new bosons (W′ and Z′) that can be part of an heavy vector triplet [6] or can be mass degenerate as a vector singlet [32,33].

The bulk graviton model is characterized by two free parameters: the mass of the first Kaluza–Klein (KK) excitation of a spin-2 boson (the KK bulk graviton), and the ratio $\tilde{\kappa} = \kappa \sqrt{8\pi}/M_{Pl}$, with κ being the unknown curvature scale of the extra dimension and M_{Pl} the Planck mass. A scenario with $\tilde{\kappa} = 0.5$ is considered in this analysis, as motivated in Ref. [34].

The HVT framework generically represents a large number of models predicting additional gauge bosons, such as the composite Higgs [35–39] and little Higgs [40,41] models. The benchmark points are formulated in terms of a few parameters: two coefficients c_F and c_H, that scale the couplings of the additional gauge bosons to fermions; to the Higgs boson and longitudinally polarized SM vector bosons, respectively, and g_V, representing the typical strength of the new vector boson interaction. For the analysis presented here, samples were simulated in the HVT model B, corresponding to $g_V = 3$, $c_H = -0.98$, and $c_F = 1.02$ [6]. For these parameters, the new resonances are narrow and have large branching fractions to vector boson pairs, while the fermionic couplings are suppressed.

All signals considered in the analysis satisfy the narrow-width approximation. The quoted results are therefore valid independent of the exact theoretical signal widths as long as the resonance widths remain smaller than the detector resolution. This makes our modelling of the detector effects on the signal shape independent of the actual model used for generating the events. All simulated samples are produced with a relative resonance width of 0.1%, in order to be within the validity of the narrow-width approximation. Monte Carlo (MC) simulated events of the bulk graviton and HVT signals are generated at leading-order (LO) in quantum chromodynamics (QCD) with MADGRAPH5_aMC@NLO versions 2.2.2 and 2.4.3 [42] and hadronization showering is simulated with PYTHIA versions 8.205 and 8.230 [43], for 2016 and 2017 detector conditions, respectively. The NNPDF 3.0 [44] LO parton distribution functions (PDFs) are used together with the CUETP8M1 [45] and CP5 [46] underlying event tunes in PYTHIA for 2016 and 2017 conditions, respectively.

Simulated samples of the SM background processes are used to optimize the analysis and create background templates, as described in Sect. 5. The QCD multijet production is simulated with four generator configurations: PYTHIA only, the LO mode of MADGRAPH5_aMC@NLO [47] matched and showered with PYTHIA, POWHEG [48–51] matched and showered with PYTHIA, and HERWIG++ 2.7.1 [52] with the CUETHS1 tune [45]. Top quark pair production is modelled at next-to-LO (NLO) with POWHEG [53], showered with PYTHIA. To calculate systematic uncertainties related to the vector boson tagging efficiency, two additional simulated samples of top quark production at LO are used: one generated with MADGRAPH5_aMC@NLO and interfaced with PYTHIA, and the second one generated and showered with PYTHIA. The production of W+jets and Z+jets (V+jets) is simulated at LO with MADGRAPH5_aMC@NLO matched and showered with PYTHIA. The same underlying event tune as for the signal samples is used for those of the background. Two corrections dependent on the transverse momentum (p_T) [54,55] are applied to the V+jets backgrounds to correct the p_T-distribution of the vector bosons computed at LO in QCD to the one predicted at NLO in QCD, and to account for electroweak effects at high p_T. The NNPDF 3.1 [56] next-to-NLO (NNLO) PDFs are employed for simulated V+jets events with the 2017 data taking conditions for both the 2016 and 2017 data analyses.

All samples are processed through a GEANT4-based [57] simulation of the CMS detector. To simulate the effect of additional pp collisions within the same or adjacent bunch

crossings (pileup), additional inelastic events are generated using PYTHIA and superimposed on the hard-scattering events. The MC simulated events are weighted to reproduce the distribution of the number of reconstructed pileup vertices observed in the 2016 and 2017 data separately.

4 Reconstruction and selection of events

4.1 Jet reconstruction

Event reconstruction is based on the particle flow (PF) algorithm [58], which reconstructs and identifies individual particles with information from the various elements of the CMS detector. Jets are reconstructed from these particles, using the anti-k_T jet clustering algorithm [59] with a distance parameter of $R = 0.8$ (AK8 jets) as implemented in the FASTJET package [60]. In order to mitigate the effect of pileup, two different algorithms are used: for 2016 data and simulation, charged particles identified as originating from pileup vertices are excluded before jet clustering begins. For 2017, we take advantage of the pileup per particle identification (PUPPI) [61] algorithm. This method uses local shape information of charged pileup, event pileup properties, and tracking information in order to rescale the four-momentum of each neutral and charged PF candidate with a weight that describes the likelihood that each particle originates from a pileup interaction. All jets are further required to pass tight jet identification requirements [62]. Jets are corrected for nonlinearities in p_T and η using jet energy corrections as described in Ref. [63]. Additionally, residual contributions from pileup are corrected using the approach outlined in Ref. [64].

Two variables are used to tag jets as potentially originating from vector boson decays to quarks for further event selection: the "groomed" mass of the jet obtained using a modified mass drop algorithm [65,66] known as soft drop [67], and the N-subjettiness ratio $\tau_{21} = \tau_2/\tau_1$ obtained with the N-subjettiness algorithm [68]. For both 2016 and 2017 data these observables are reconstructed from AK8 jets with PUPPI pileup mitigation applied, decreasing their dependence on pileup as shown in Ref. [62], while the overall jet four-momenta are calculated using the pileup mitigation algorithms as described above.

The groomed jet mass is calculated using the soft drop algorithm, with angular exponent $\beta = 1$, soft cutoff threshold $z_{cut} < 0.1$, and characteristic radius $R_0 = 0.8$ [67], which is applied to remove soft, wide-angle radiation from the jet. This is a generalization of the "modified mass" drop tagger algorithm [65,66], and the two are identical when the angular exponent $\beta = 0$. This algorithm is based on reclustering the constituents of the AK8 jets using the Cambridge–Aachen algorithm [69,70]. The soft drop jet mass m_{jet}, calculated as the invariant mass of the four-momenta sum of the

final remaining jet constituents, weighted according to the PUPPI algorithm, is utilized in the offline analysis and will be denoted as jet mass in the following. The mass is corrected for p_T- and η-dependent nonuniformities due to detector effects, following the procedure described in Ref. [62].

This algorithm is used for the offline analysis, while the jet-trimming algorithm [71] is used at trigger level, see Sect. 4.2. The jet-trimming algorithm reclusters each AK8 jet starting from all its original constituents using the k_T algorithm [72] to create subjets with a size parameter R_{subjet} set to 0.2, discarding any subjet with $p_T^{subjet}/p_T^{jet} < 0.03$.

The N-subjettiness variable, τ_N, is defined as

$$\tau_N = \frac{1}{r_0} \sum_k p_{T,k} \min(\Delta R_{1,k}, \Delta R_{2,k}, \ldots, \Delta R_{N,k}), \quad (1)$$

where the index k runs over the PF constituents of the jet, and the distances $\Delta R_{n,k}$ are calculated relative to the axis of the n-th subjet. The normalization factor r_0 is calculated as $r_0 = R_0 \sum_k p_{T,k}$, setting R_0 to the distance parameter used in the clustering of the original jet. The variable τ_N quantifies the compatibility of the jet clustering with the hypothesis that exactly N subjets are present, with small values of τ_N indicating greater compatibility. The ratio between 2- and 1-subjettiness, $\tau_{21} = \tau_2/\tau_1$, is found to be a powerful discriminant between jets originating from V decays into quarks (V boson jets) and jets developed from prompt quarks and gluons (quark/gluon jets). Jets from W or Z decays in signal events are characterized by lower values of τ_{21} relative to SM backgrounds. However, the τ_{21} variable shows a dependence on the jet p_T-scale as well as the jet mass. This particularly affects the monotonically falling behaviour of the nonresonant background distributions. Since this search probes a large range of jet masses and dijet invariant masses (m_{jj}), we decorrelate τ_{21} from the jet p_T-scale and jet mass following the "designed decorrelated taggers (DDT)" methodology presented in Ref. [73]. We thereby reduce the τ_{21} profile dependence on $\rho' = \ln(m_{jet}^2/(p_T \mu))$, where $\mu = 1\,\text{GeV}$. This leads to the following definition of τ_{21}^{DDT}:

$$\tau_{21}^{DDT} = \tau_{21} - M \rho', \quad (2)$$

where M is the extracted slope from a fit to the τ_{21} profile versus ρ' in QCD multijet events simulated with PYTHIA after applying the full analysis selections. It is evaluated to be $M = -0.080$. The τ_{21} (upper) and τ_{21}^{DDT} (lower) profile dependencies on ρ' are shown in Fig. 1. We observe a small residual difference between intervals of p_T, but this has a negligible impact on the analysis.

We observe a significant gain in analysis sensitivity when using τ_{21}^{DDT}. Since this variable is a function of both N-subjettiness and the ratio of jet mass and transverse momentum, it leads to a larger separation between signal and back-
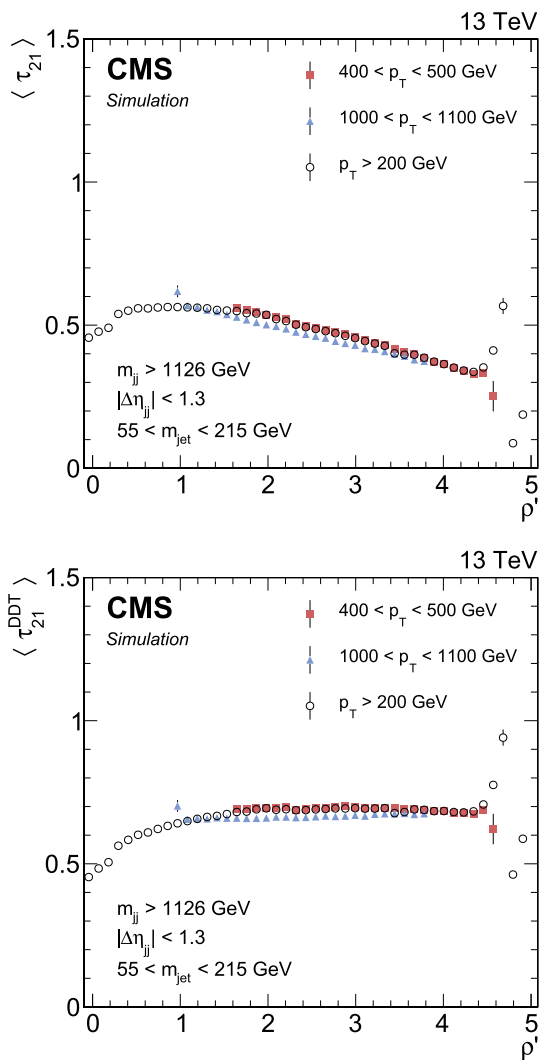
Fig. 1 The τ_{21} (upper) and τ_{21}^{DDT} (lower) profile dependencies on $\rho' = \ln(m_{\mathrm{jet}}^2/(p_{\mathrm{T}}\mu))$ examined in QCD multijet events simulated with PYTHIA. A fit to the linear part of the spectrum for $p_{\mathrm{T}} > 200\,\mathrm{GeV}$ yields the slope $M = -0.080$, which is used to define the mass- and p_{T}-decorrelated variable $\tau_{21}^{\mathrm{DDT}} = \tau_{21} - M\,\rho'$

ground as shown in the comparison of τ_{21}^{DDT} and τ_{21} in Fig. 2 (upper). Furthermore, using the τ_{21}^{DDT} variable reduces the dependency of m_{jet} on m_{jj}, leading to smoothly falling distributions in the jet mass as shown in Fig. 2 (lower).

4.2 Trigger and preliminary offline selection

Events are selected online with a variety of different jet triggers based on the highest jet p_{T} or the p_{T} sum of all jets in the event (H_{T}). For some of these triggers additional requirements on the trimmed mass are applied in order to be able to lower the p_{T} and H_{T} thresholds. For example, for 2017 data taking, requiring the trimmed jet mass of the leading-p_{T} jet to be above 30 GeV allows the lowering of the p_{T} threshold
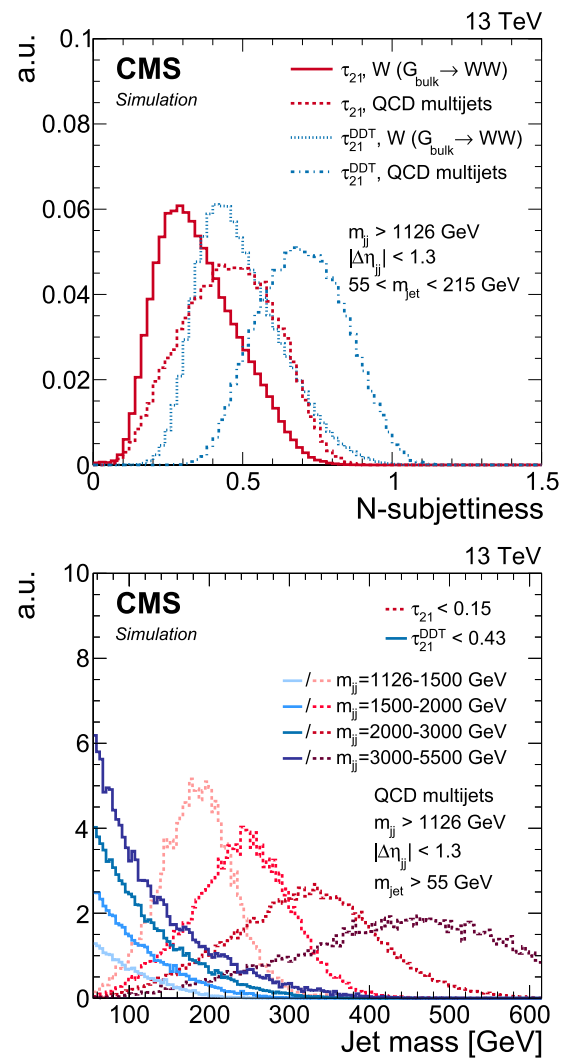
Fig. 2 Distribution of the N-subjettiness discriminants (τ_{21} and τ_{21}^{DDT}) for W-jets and quark/gluon jets from QCD multijet events (upper). Distributions in the jet mass of QCD multijet events for four m_{jj} bins in the range 1126–5500 GeV after a cut on τ_{21} and τ_{21}^{DDT} corresponding to the same mistag rate of about 2% (lower). For both discriminants, darker colours correspond to higher m_{jj} ranges. The distributions are arbitrarily scaled for better readability. The analysis selections applied to derive these distributions are specified in the plots. For this analysis the working point of $\tau_{21}^{\mathrm{DDT}} \leq 0.43$ is chosen

from 500 to 360 GeV while maintaining a similar rate. In the case of the H_{T}-triggers, the threshold can be lowered from 1050 to 750–800 GeV when requiring a trimmed jet mass greater 50 GeV. The H_{T}-triggers utilize a standard jet collection of anti-k_{T} jets with a distance parameter $R = 0.4$, while the triggers based on the trimmed jet mass operate on AK8 jets. The triggers used for the 2017 data set are conceptually similar to those used in 2016, and correspond to those used in Ref. [29]. The 2017 trigger thresholds were slightly greater than those in 2016 in order to maintain the same trigger rate despite a higher instantaneous luminosity.
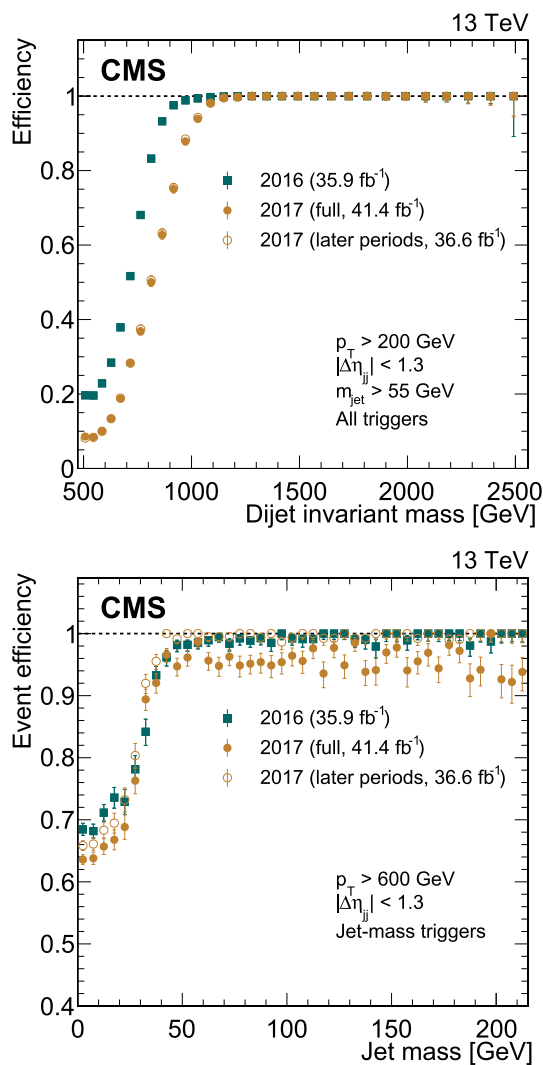
Fig. 3 The trigger efficiency as a function of the dijet invariant mass for a combination of all triggers used in this analysis (upper) and the event efficiency for either of the selected jets to pass triggers requiring an online trimmed mass of at least 30 GeV as a function of the jet mass (lower). The solid yellow circles correspond to the trigger efficiencies for the full 2017 data set and do not reach 100% efficiency because the jet mass based triggers were unavailable for a period at the beginning of data taking (corresponding to 4.8 fb^{-1}). The open yellow circles are the corresponding efficiencies excluding this period. The uncertainties shown are statistical only

The trigger efficiency as a function of the dijet invariant mass is measured in an orthogonal single muon data set, shown in Fig. 3, using a combination of all triggers (upper), and as a function of the jet mass for the triggers exploiting the trimmed jet mass (lower). For the trimmed jet mass triggers, the efficiency plateau as a function of the jet mass does not reach 100% for the full 2017 data set (full yellow circles), since these triggers were not used for the first 4.8 fb^{-1} of data recorded. The trigger efficiency excluding this period is shown with open yellow circles. The combination of all trig-

gers is > 99% efficient above dijet invariant masses of 990 and 1126 GeV for the full 2016 and 2017 data sets, respectively. For simplicity, the subsequent analysis requires the dijet invariant mass to be above 1126 GeV for both data sets. Given the m_{jj} resolution of about 10%, the lowest resonance mass that is accepted with high efficiency by the analysis is 1.2 TeV.

All events are required to have at least one primary vertex reconstructed within a 24 cm window along the beam axis, with a transverse distance from the average pp interaction region of less than 2 cm [74]. The reconstructed vertex with the largest value of summed physics-object p_T^2 is taken to be the primary pp interaction vertex. The physics objects are the jets, clustered using the jet finding algorithm [59,60] with the tracks assigned to the vertex as inputs, and the associated missing transverse momentum, taken as the negative vector sum of the p_T of those jets.

4.3 Event selection

Events are selected by requiring at least two jets with $p_T > 200$ GeV and $|\eta| < 2.5$. The two jets with the highest p_T in the event are selected as potential vector boson candidates and are required to have a separation of $|\Delta\eta| < 1.3$ in order to reduce the QCD multijet background. In addition to the requirement that the two jets invariant mass $m_{jj} > 1126$ GeV, based on the trigger selection discussed above, it is further required that $m_{jj} < 5500$ GeV. The upper cut on mjj is well above the highest dijet mass event observed in data. To simplify the modelling of the 3D shapes in the $m_{jj}-m_{jet1}-m_{jet2}$ space, the two jets are labelled at random so that the mass distributions of the first and second selected jet, m_{jet1} and m_{jet2}, have the same shape. Jets originating from the misreconstruction of a high momentum lepton are rejected by requiring an angular separation $\Delta R > 0.8$ to muons (electrons) with p_T greater than 20 (35) GeV and satisfying identification criteria optimized for high-momentum leptons [75,76]. To reduce the QCD multijet background, we require the jet mass to be between 55 and 215 GeV. The selected events are further grouped into two categories according to their likelihood to originate from a boson decay into quarks, as quantified by τ_{21}^{DDT}. The jet mass, τ_{21}^{DDT}, and dijet invariant mass distributions for data and simulation are shown in Fig. 4.

In the high-purity (HPHP) category, both jets are required to have $0 < \tau_{21}^{DDT} \leq 0.43$, while in the low-purity (HPLP) category only one of the jets needs to fulfill this requirement, and the other must satisfy $0.43 < \tau_{21}^{DDT} \leq 0.79$. These conditions yield the highest expected signal significance over the whole mass range, while at the same time selecting at least 95% of the signal. The addition of the HPLP category improves the expected cross section upper limit by around 20% at high dijet invariant mass where the background is low. Finally, a loose requirement of $\rho = \ln(m_{jet}^2/p_T^2) < -1.8$ is
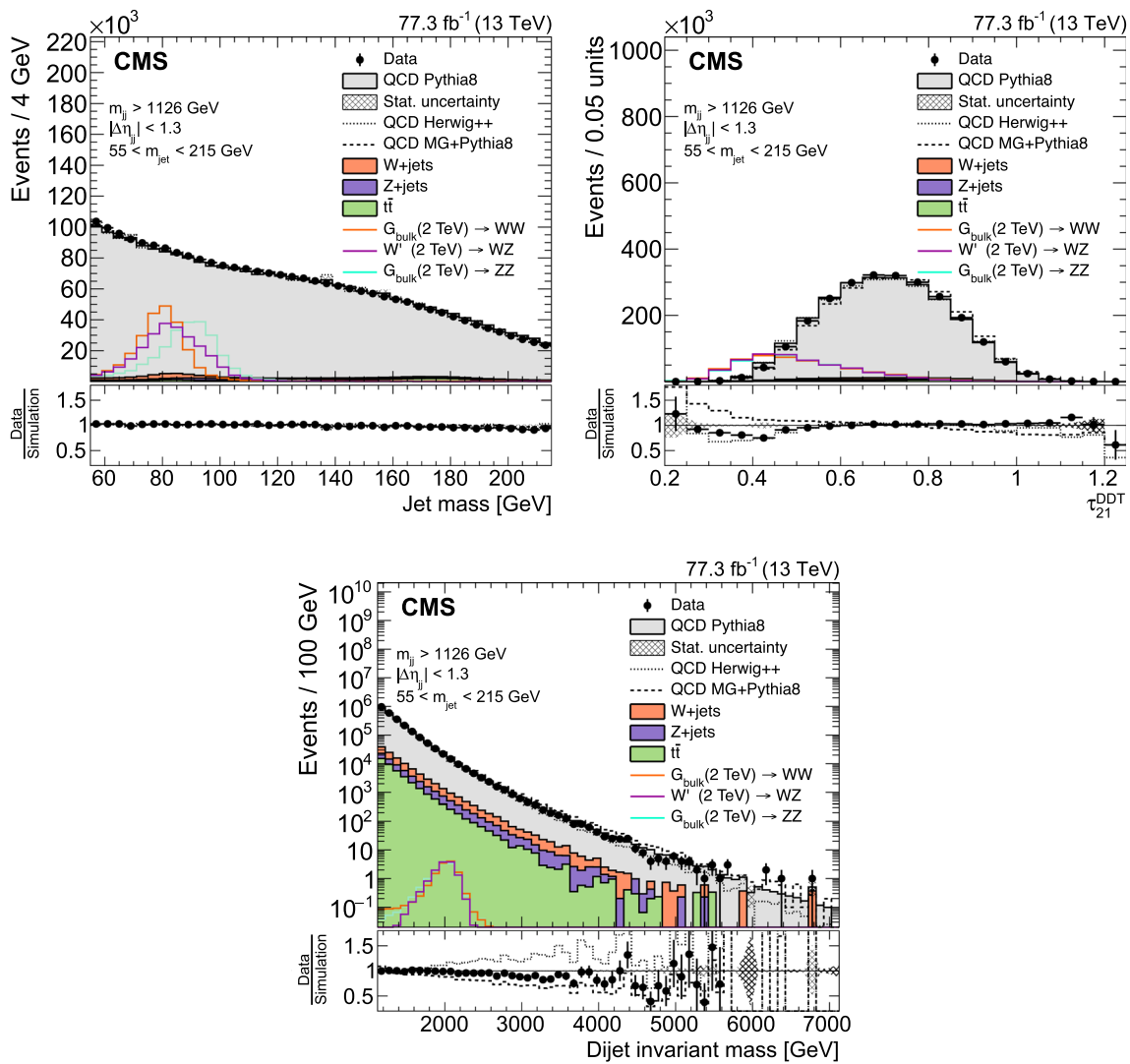
Fig. 4 Jet mass (upper left) and τ_{21}^{DDT} (upper right) distributions for selected jets (one random jet per event), and dijet invariant mass distribution (lower), for events with a jet mass between 55 and 215 GeV. For the QCD multijet simulation, several alternative predictions are shown, scaled to the data minus the other background processes, which are scaled to their SM expectation as described in the text. The different signal distributions are scaled to be visible. No selection on τ_{21}^{DDT} is applied. The ratio plots show the fraction of data over QCD multijet simulation for PYTHIA8 (black markers), HERWIG++ (dotted line), and MADGRAPH+PYTHIA8 (dashed line)

applied in order to veto events in which the jet mass is high, but the jet p_{T} is low. In these cases the cone size of $\Delta R = 0.8$ is too small to contain the full jet, affecting both the jet mass resolution and the τ_{21}^{DDT} tagging efficiency, which is not well modelled in simulation. This selection has a negligible effect on the signal, which typically has jets with masses around the W or Z boson mass and high p_{T}.

4.4 Substructure variable corrections and validation

Figure 4 shows a notable deviation in the shape of the τ_{21}^{DDT} distribution between data and simulation. Such mismodelling introduces a bias in the jet tagging efficiency

for the signal, and as a consequence in the measured signal rate. We therefore compute scale factors to correct the signal efficiency accordingly. For the background jets, this mismodelling requires no further correction, because of the data-driven approach adopted in this analysis, where the background shape and normalization are fitted to data with large pre-fit uncertainties as described in the following sections.

The W boson tagging scale factors and jet mass scale and resolution uncertainties are estimated from data by isolating a control sample of merged W bosons in a high-p_{T} $t\bar{t}$ sample. This is done by performing a simultaneous fit to the jet mass distributions for the two ranges of τ_{21}^{DDT}, as detailed in

Table 1 The W jet mass peak position (m) and resolution (σ), and the W-tagging efficiencies, as extracted from top quark enriched data and from simulation, together with the corresponding data-to-simulation scale factors. The uncertainties in the scale factors include systematic uncertainties estimated as described in Ref. [62]

	m [GeV]	σ [GeV]	W-tagging efficiency
2016			
$\tau_{21}^{\mathrm{DDT}} < 0.43$			
Data	82.0 ± 0.5 (stat)	7.1 ± 0.5 (stat)	0.080 ± 0.008 (stat)
Simulation	80.9 ± 0.2 (stat)	6.6 ± 0.2 (stat)	0.085 ± 0.003 (stat)
Data/simulation	1.014 ± 0.007 (stat + syst)	1.09 ± 0.09 (stat + syst)	0.94 ± 0.10 (stat + syst)
$0.43 < \tau_{21}^{\mathrm{DDT}} < 0.79$			
Data			0.920 ± 0.008 (stat)
Simulation			0.915 ± 0.003 (stat)
Data/simulation			1.006 ± 0.009 (stat + syst)
2017			
$\tau_{21}^{\mathrm{DDT}} < 0.43$			
Data	80.8 ± 0.4 (stat)	7.7 ± 0.4 (stat)	0.065 ± 0.006 (stat)
Simulation	82.2 ± 0.3 (stat)	7.1 ± 0.3 (stat)	0.068 ± 0.005 (stat)
Data/simulation	0.983 ± 0.007 (stat + syst)	1.08 ± 0.08 (stat + syst)	0.96 ± 0.12 (stat + syst)
$0.43 < \tau_{21}^{\mathrm{DDT}} < 0.79$			
Data			0.935 ± 0.006 (stat)
Simulation			0.932 ± 0.005 (stat)
Data/simulation			1.003 ± 0.008 (stat + syst)

Ref. [62]. To extract the efficiency from a clean sample of merged W bosons, the $\mathrm{t\bar{t}}$ sample is split into two components, depending on whether the quarks from the W boson decay at truth level are within $\delta R = 0.8$ or not, i.e. on whether the hadronic boson decay is merged into a single jet or not. Only the merged component is considered in the efficiency calculation and the mass scale and resolution extraction.

The efficiencies and scale factors obtained are listed in Table 1 for 2016 and 2017 data, with the corresponding fits shown in Fig. 5. The W boson tagging efficiency in the selected $\mathrm{t\bar{t}}$ events of around 7% is relatively low compared to the efficiency in signal events, since these events are dominated by W boson jets with a p_T of around 200 GeV, just at the threshold where the decay products of the W boson merge into a single jet. The signal jets, however, mostly have a p_T above 600 GeV, and a tagging efficiency around 35%. The signal efficiency for τ_{21}^{DDT} increases with the jet p_T, whereas the background efficiency is constant, as shown in Ref. [62]. Two systematic uncertainties in the scale factors are added: one due to differences in MC generation and modelling of the parton shower and one due to NNLO corrections. The former is evaluated by comparing the resulting scale factors when using $\mathrm{t\bar{t}}$ simulation produced with different generators. The latter is evaluated by comparing the extracted efficiencies with and without reweighting according to the top quark p_T, where the reweighting is derived from data in order to better describe the observed p_T distribution in $\mathrm{t\bar{t}}$ data [77]. The jet mass scale and resolution are estimated in the same fits and also listed in Table 1. The difference in jet mass scale between data and simulation is around 2%, and the jet mass

resolution difference is roughly 8%. These are used to scale and smear the jet mass in simulation, and their uncertainties are additionally inserted as systematic uncertainties in the final fit.

5 The multi-dimensional fit

The background estimation technique used in previous versions of this analysis [7,10,29] relied on a one-dimensional (1D) fit of the dijet invariant mass after a tight jet mass selection (65–105 GeV) has been applied. In the analysis presented here, we take advantage of the fact that the signal peaks in three observables (the jet masses m_{jet1} and m_{jet2}, and the dijet invariant mass m_{jj}), and attempt to extract the signal by searching for peaks in the multi-dimensional m_{jj}–m_{jet1}–m_{jet2} space. This method permits searches for generic resonances, decaying to two SM or non-SM bosons, anywhere in the jet mass and dijet invariant mass spectra in the future. Additionally, tight jet mass cuts as used in previous diboson resonance searches are no longer needed, as we fit the full jet mass line shape to extract the signal. Since such a cut around the vector boson mass leads to about 20% inefficiency for the W and Z boson signals, including all the events that would fall outside the mass window reduces the statistical uncertainties in the fitting procedure. Furthermore, the background m_{jj} shape is better constrained at high dijet invariant masses than it is in the previous method.

Fitting the jet mass and resonance mass together also allows us to add nuisance parameters that simultaneously
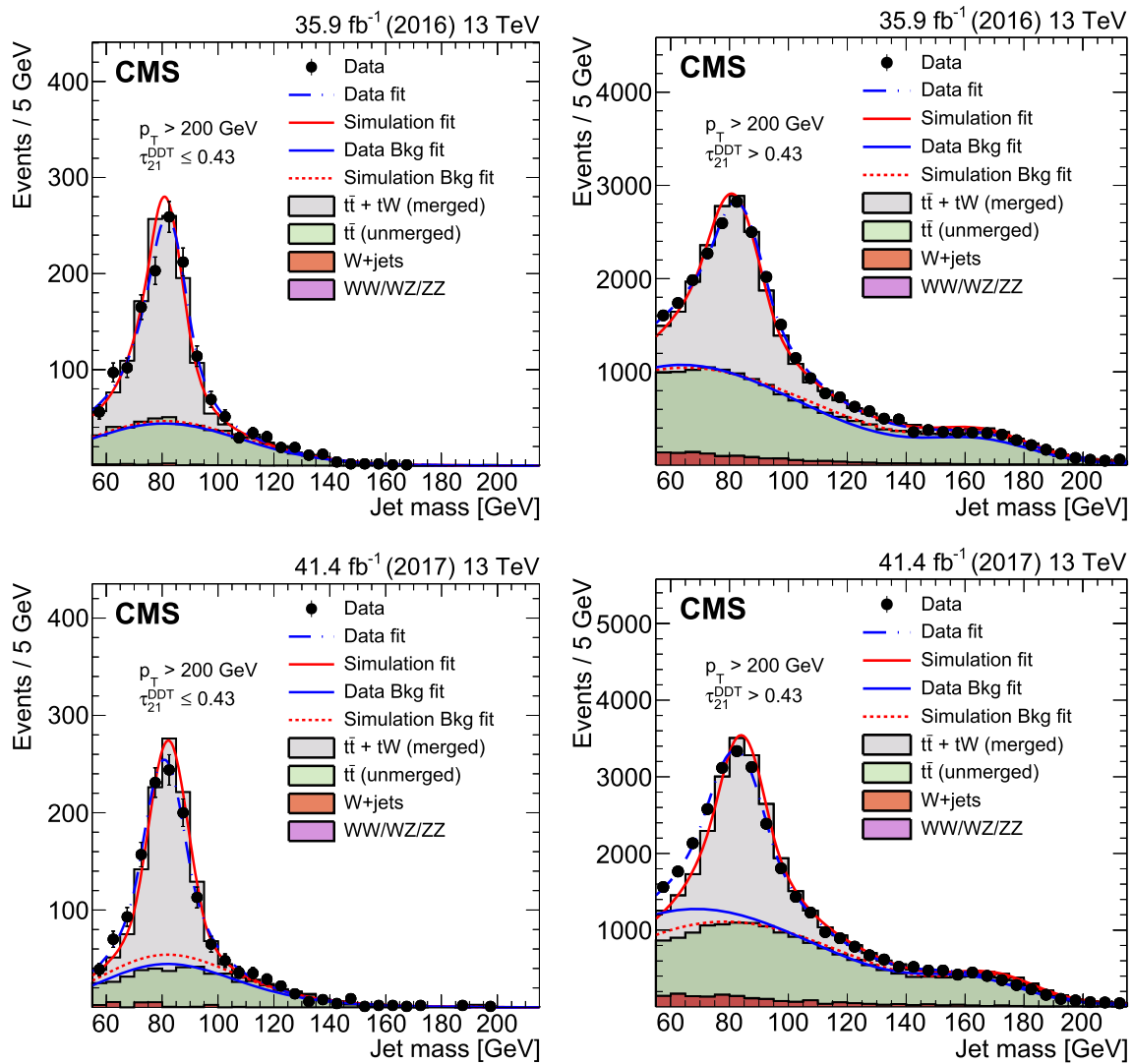
Fig. 5 The jet mass distribution for events that pass (left) and fail (right) the $\tau_{21}^{\mathrm{DDT}} \leq 0.43$ selection in the $t\bar{t}$ control sample. The results of the separate fits to data and to simulation are shown by the dash-dotted blue and solid red lines, respectively. The background components of the fits are shown as dashed and dash-dotted lines. The fit to 2016 data is shown in the upper panels and the fit to 2017 data in the lower panels. The associated uncertainties are shown in Table 1 and discussed further in Sect. 4.4

affect the jet masses and the resonance mass, accounting for their correlation. We build a three dimensional background model starting from simulation. As the number of simulated events is small, a forward-folding kernel approach is used to ensure a full and smooth model, as described in Sect. 5.2.1. Further, to account for discrepancies in the QCD multijet background simulation and data, we allow the background model to adapt to the data using physically motivated shape variations.

The random jet labelling adapted in the analysis results in essentially the same jet mass distributions for jet-1 and jet-2 in the modelling and removes any correlations between the two jet masses. Thus only the distribution for one of the jet masses are shown in the following figures.

5.1 Signal modelling

For each mass point m_{X} and each purity category, the signal yield per pb of cross section is calculated as the integral of the histogram produced from the parameterization. The total signal yield for events passing all analysis selections divided by the number of generated events as a function of m_{X} is shown in Fig. 6.

The signal shape in three dimensions is defined as a product of the shape of the resonance mass and the jet masses:

$$P_{\mathrm{sig}}(m_{\mathrm{jj}}, m_{\mathrm{jet1}}, m_{\mathrm{jet2}} | \overline{\theta}^{\mathrm{s}}(m_{\mathrm{X}})) = P_{\mathrm{VV}}(m_{\mathrm{jj}} | \overline{\theta}_1^{\mathrm{s}}(m_{\mathrm{X}}))$$
$$\times P_{\mathrm{j1}}(m_{\mathrm{jet1}} | \overline{\theta}_2^{\mathrm{s}}(m_{\mathrm{X}})) \, P_{\mathrm{j2}}(m_{\mathrm{jet2}} | \overline{\theta}_3^{\mathrm{s}}(m_{\mathrm{X}})).$$
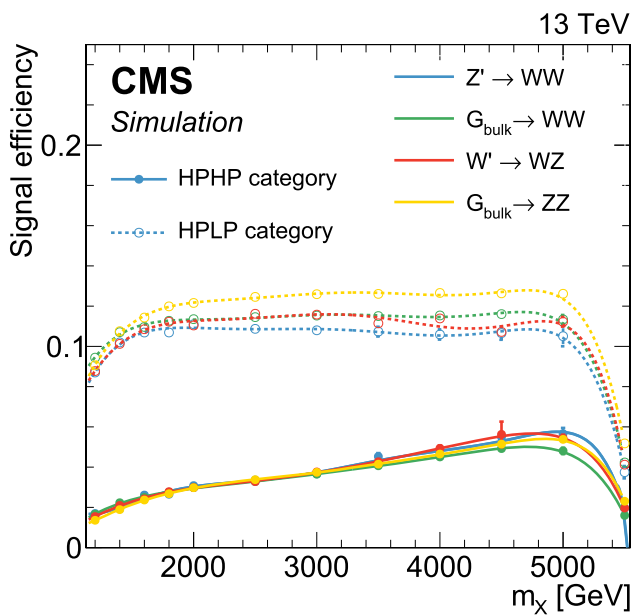
Fig. 6 Total signal efficiency as a function of m_X after all selections are applied, for signal models with a Z' decaying to WW, G_{bulk} decaying to WW, W' decaying to WZ, and G_{bulk} decaying to ZZ. The denominator is the number of generated events. The solid and dashed lines show the signal efficiencies for the HPHP and HPLP categories, respectively. The decrease in efficiency between 5.0 and 5.5 TeV is due to the requirement $m_{jj} < 5500\,\mathrm{GeV}$

The shapes for m_{jj}, m_{jet1}, and m_{jet2} are parameterized independently as a function of the hypothesized mass (m_X) of a new particle and a set of general probability density function (pdf) parameters $\overline{\theta}^s = (\overline{\theta}_1^s, \overline{\theta}_2^s, \overline{\theta}_3^s)$ that depend on m_X. The parameters $\overline{\theta}^s$ denote for instance the mean and width of the analytic function chosen to model the signal distributions. The m_{jet} and m_{jj} distributions can be treated as uncorrelated since correlations are found to be negligible for the signal. The signal is parameterized by fitting the simulated resonance mass and jet mass line shapes for each m_X, extracting the quantities, and then interpolating these to intermediate values of the resonance mass. P_{j1} and P_{j2} are fitted and parameterized separately from each other using different sets of $\overline{\theta}^s$, although they are effectively identical because of the random jet labelling. For the parameterization of the resonance mass m_{jj} and the m_{jet} masses, double-sided Crystal Ball (dCB) functions [78] are used for each m_X. Each parameter of the dCB is interpolated between different resonance masses using polynomials of a degree sufficient to ensure a smooth shape interpolation for all resonance masses. The resulting signal shapes for all signal models are shown in Fig. 7 for the dijet invariant mass (upper) and the mass of jet-1 in the HPHP category (lower). Because of the random jet labelling the distribution for jet-2 is effectively identical to that shown for jet-1. The jet mass scale and resolution as a function of the dijet invariant mass are extracted from the
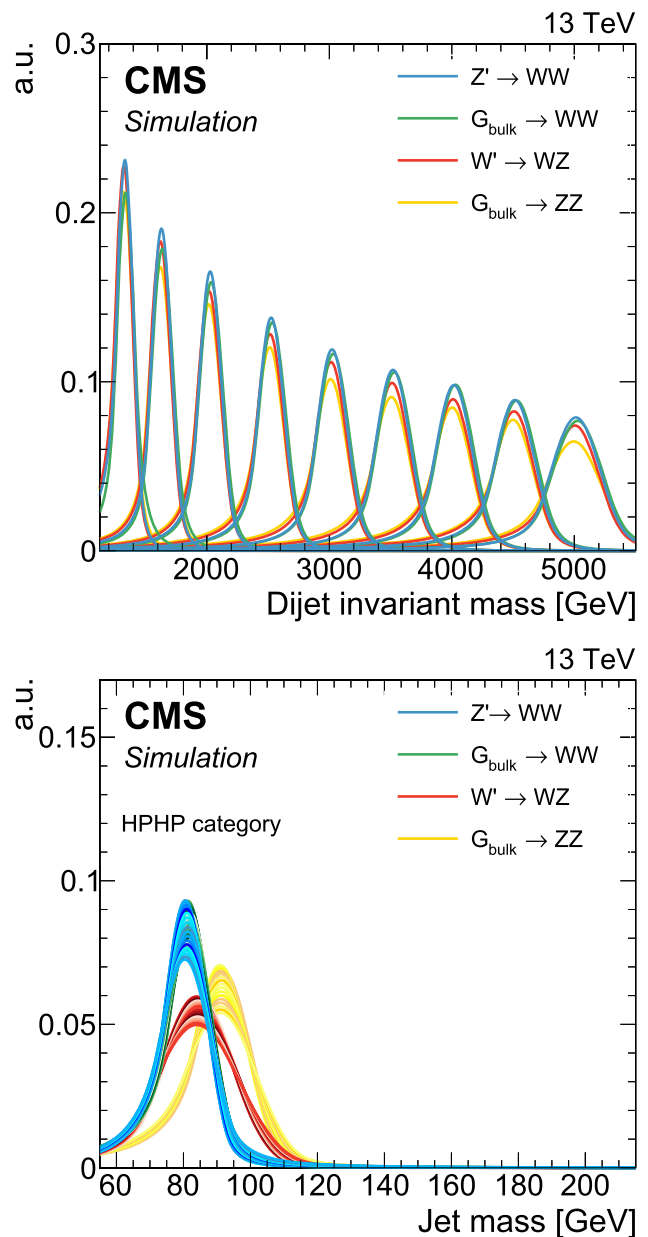

Fig. 7 The final m_{jj} (upper) and m_{jet1} (lower) signal shapes extracted from the parameterization of the dCB function. The same m_{jj} shapes are used for both purity categories. The jet mass distributions are shown for a range of resonance masses between 1.2 and 5.2 TeV for one of the two jets in the events in the HPHP category. Because the jets are labelled randomly, the jet mass distributions for the second jet are essentially the same as the one shown. The distributions for a G_{bulk} decaying to WW have the same shapes as those for the Z' signal and are therefore not visible

mean and width of the dCB function. The mass scale and resolution are shown in Fig. 8 after the full HPHP (HPLP) analysis selections have been applied. The jet mass resolution increases about 3% from the lowest to the highest resonance mass, while its scale is found to be stable. The mean of the
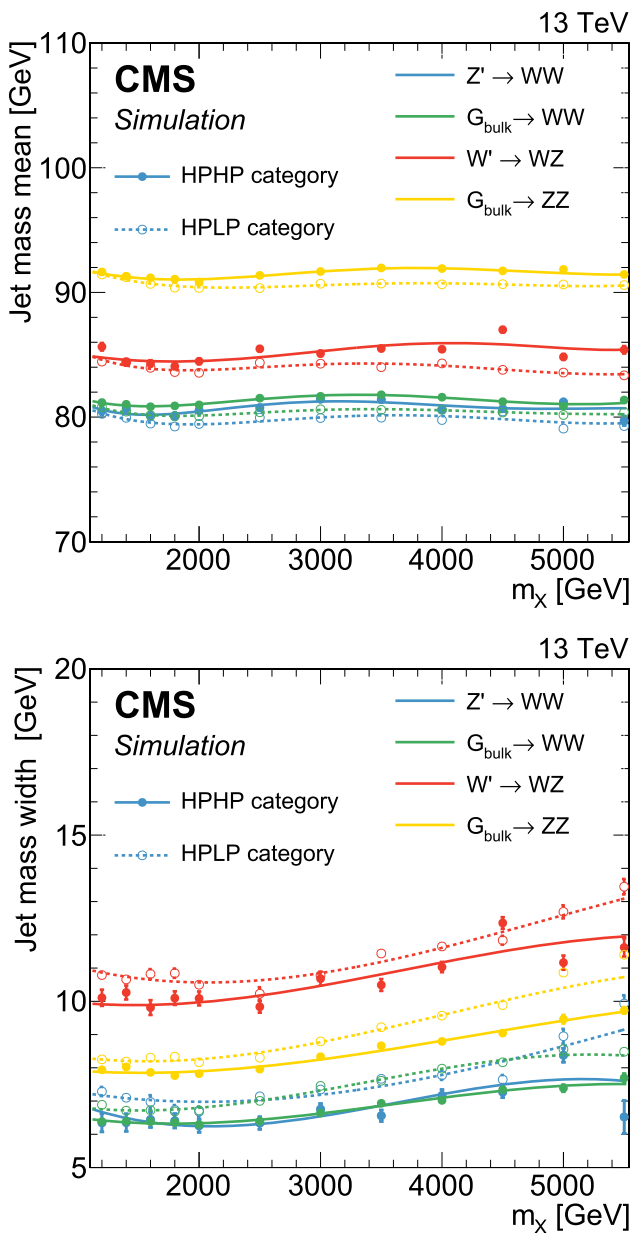
Fig. 8 The mass scale (upper) and resolution (lower) of the jet as a function of m_X, obtained from the mean and width of the dCB function used to fit the jet mass spectrum. The HPHP (solid lines) and HPLP (dotted lines) categories are shown for different signal models. The distributions are only shown for one of the two jets in the event, since the distributions for the second jet are essentially the same

dijet invariant mass distributions is consistent with the mass of the resonance m_X, as seen in Fig. 7 upper.

5.2 Background modelling

5.2.1 Nonresonant background

As mentioned above, previous versions of this analysis estimate the QCD multijet background by a parametric fit to

the data in the m_{jj} signal region. The fit is well-constrained by highly populated bins with small statistical uncertainties at low m_{jj}, but is less constrained for high values of m_{jj}. This method allows the incorporation of additional information in the fit by modelling the correlations between the jet mass and the dijet invariant mass for SM background processes, which were not explicitly studied in the past. It is important to note that the correlations between m_{jet} and m_{jj} have to be modelled for the QCD multijet background, as opposed to the signals negligible correlations due to its localization in the three-dimensional space. In this analysis, we build a three dimensional background model starting from simulation. Since the size of the simulated samples is limited, we start from particle-level information and use a "forward-folding" kernel approach that is similar to the technique presented in Ref. [79] and used in Ref. [11]. Finally, we incorporate sufficient nuisance parameters into the fit to account for any discrepancies between data and simulation. In order to model the QCD multijet background in the 3D m_{jj}–m_{jet1}–m_{jet2} hyperplane, we use the following conditional product:

$$P_{QCD}(m_{jj}, m_{jet1}, m_{jet2}|\overline{\theta}^{QCD}) = P_{VV}(m_{jj}|\overline{\theta}_1^{QCD})$$
$$\times P_{cond,1}(m_{jet1}|m_{jj}, \overline{\theta}_2^{QCD}) \, P_{cond,2}(m_{jet2}|m_{jj}, \overline{\theta}_3^{QCD}).$$

Since the jet mass is correlated with the jet p_T for the QCD multijet background, its shape is required to be modelled conditionally as a function of m_{jj} for both jets. Two two-dimensional (2D) templates (denoted as $P_{cond,1}$ and $P_{cond,2}$) are modelled for the two jet masses separately, containing different jet mass shapes in bins of m_{jj}. The m_{jj} distribution is computed as a 1D pdf. The parameter sets denoted by $\overline{\theta}^{QCD}$ represent the nuisance parameters in each pdf.

To build the 2D conditional templates, $P_{cond,1}$ and $P_{cond,2}$, each available particle-level event is smoothed with a 2D Gaussian kernel, where each 2D kernel links the particle-level event quantities to the reconstruction level. Thus each simulated event contributes a smoothed Gaussian shape to the total conditional pdf. The Gaussian kernel depends on the dijet invariant mass scale and resolution, as well as the jet mass scale and resolution. The m_{jet} and m_{jj} scale and resolution are extracted from a Gaussian fit to either $m_{jet}(reco)/m_{jet}(gen)$ or $m_{jj}(reco)/m_{jj}(gen)$, in bins of particle-level jet p_T.

The mass scale and resolution are then used to populate the conditional 2D histogram. Each generated event i is smeared with a 2D Gaussian kernel,

$$k(m_{jet}, m_{jj}) = \frac{w_i}{2\pi r_{m_{jj},i} r_{m_{jet},i}}$$
$$\times \exp\left[-\frac{1}{2}\left(\frac{m_{jj} - s_{m_{jj},i}}{r_{m_{jj},i}}\right)^2 - \frac{1}{2}\left(\frac{m_{jet} - s_{m_{jet},i}}{r_{m_{jet},i}}\right)^2\right],$$
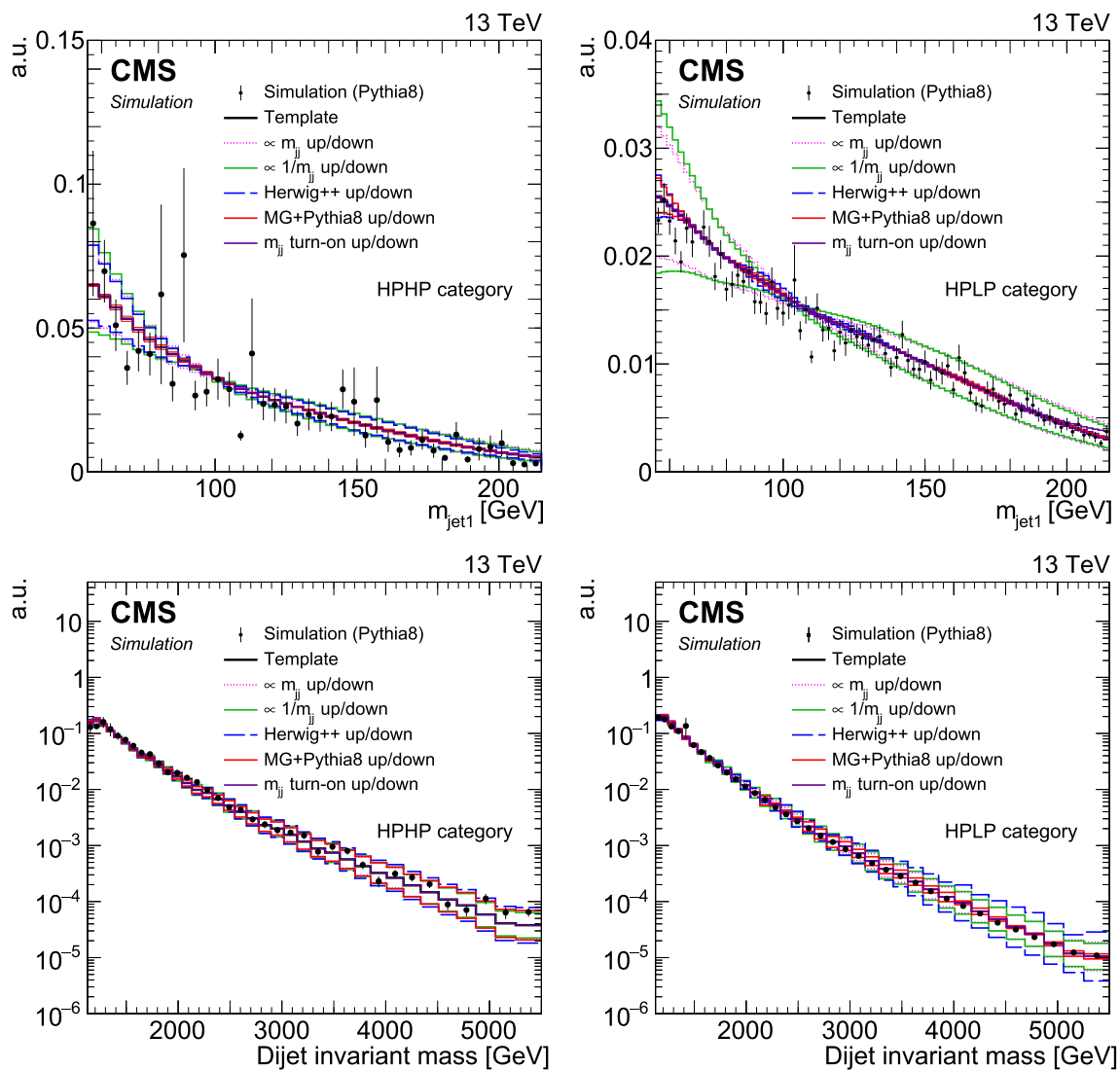
Fig. 9 Nominal QCD multijet simulation using PYTHIA8 (data points) and three-dimensional pdfs derived using a forward-folding kernel approach (black solid line), shown together with the five alternate shapes that are added to the multi-dimensional fit as shape nuisance parameters. The shapes for the high-purity (left) and low-purity (right) categories obtained with the 2017 simulation are shown for the projection on m_{jet1} (upper) and m_{jj} (lower). The projection on m_{jet2} is omitted since it is equivalent to the m_{jet1} projection except for statistical fluctuations. The pdfs and the simulations shown are normalized to unity. The normalization uncertainty of 50% is not shown. The distributions for 2016 simulations are similar

where s_i and r_i are the scale and the resolution derived in the previous step, and w_i is a product of event weights accounting for the normalization effects such as the individual sample production cross sections. In this way, the jet mass in generated events is scaled and smeared according to the evaluated scale and resolution, and a 2D histogram is filled with smooth Gaussian shapes. According to this procedure the jet mass (m_{jj}) resolution is about 7–10% (3–7%) of the mass of the generated jet, depending on its p_{T}. This procedure is performed separately for m_{jet1} and m_{jet2} however the two resulting templates $P_{\text{cond},1}$ and $P_{\text{cond},2}$ are essentially the same because of the random jet labels. Finally, we interpo-late the 2D histogram in order to have valid values of the pdf in all m_{jj} bins. Starting from the histogram, coarsely binned in m_{jj}, for each m_{jet} bin a spline is fitted over all m_{jj} bins. The spline is then used to interpolate values of the histogram for all final m_{jj} bins, resulting in a 2D histogram with the desired binning.

To build the 1D template for the dijet invariant mass, P_{VV}, a 1D Gaussian kernel is constructed starting from particle-level quantities where, for each MC event, a Gaussian probability distribution, rather than a single point representing the mean, contributes to the total 1D pdf using the same procedure as for the 2D templates.

Table 2 Summary of the systematic uncertainties and their impact the affected quantities. Numbers in parentheses correspond to uncertainties for the 2016 analysis if these differ from those for 2017. Dashes indicate shape variations that cannot be described by a single parameter, and are discussed in the text

Source	Relevant quantity	HPHP unc. (%)	HPLP unc. (%)
PDFs	Signal yield	3	
W boson tagging efficiency	Signal + V + jets yield	25 (21)	13 (11)
W boson tagging p_T dependence	Signal + V + jets yield	8–23	9–25
Integrated luminosity	Signal + V + jets yield	2.3 (2.6)	
QCD normalization	Background yield	50	
W+jets normalization	Background yield	20	
Z+jets normalization	Migration	20	
PDFs	Signal m_{jj}/m_{jet} mean and width	< 1	
Jet energy scale	Signal m_{jj} mean	2	
Jet energy resolution	Signal m_{jj} width	5	
Jet mass scale	Signal + V + jets m_{jet} mean	2	
Jet mass resolution	Signal + V + jets m_{jet} width	8	
QCD HERWIG++	QCD shape	–	
QCD MADGRAPH+PYTHIA8	QCD shape	–	
p_T variations	QCD shape	–	
Scale variations	QCD shape	–	
High-m_{jet} turn-on	QCD shape	–	
p_T variations	V + jets m_{jj} shape	–	

Because of the low number of events in the HPHP category, the 3D kernel derived in the HPLP category, which has a similar shape, is used to model the HPHP background. This is done by adapting the templates derived in the HPLP category to the HPHP category in the QCD multijet simulation through a fit, and then by using the corresponding post-fit distribution as the nominal template for the HPHP category. The free parameters in the fit are the alternate shapes proportional to m_{jj}, m_{jet}, $1/m_{jj}$, and $1/m_{jet}$, as listed in Sect. 6. The projections on the three different axes of the final 3D pdf, in bins of m_{jj} or m_{jet}, are shown in Fig. 9, compared to the spectra obtained using bare QCD multijet simulation events. Good agreement is observed, and any residual discrepancies are covered by the systematic shape uncertainties described in Sect. 6 and also shown in Fig. 9. Repeating the template building process and performing fits to a control region in data where both jets fail the high-purity requirement confirms the validity of this approach. In addition, the adaptability of the method was further confirmed by fitting a QCD multijet background generated at NLO with POWHEG.

5.2.2 Resonant background

The resonant background is defined as all SM processes containing at least one jet originating from a genuine W or Z boson decay. It is dominated by V+jets events, with a minor contribution from $t\bar{t}$ production and an inconsequential contribution from SM VV production, that is absorbed into the V+jets modelling. As the labelling of each jet is arbitrary,

each jet mass distribution contains two contributions: a resonant part consisting of genuine vector-boson jets, peaking around the W or Z boson mass; and a nonresonant part, composed of mistagged jets originating from a prompt quark or a gluon. These two contributions are modelled separately for each jet mass dimension. A 3D pdf for the resonant backgrounds, P_{V+jets}, is built as a product of three 1D pdfs as follows:

$$P_{V+jets}\left(m_{jet1}, m_{jet2}, m_{jj}|\bar{\theta}\right) = 0.5\left(P_{VV}(m_{jj}|\bar{\theta}_1)\right.$$
$$\times P_{res}(m_{jet1}|\bar{\theta}_2) P_{nonres}(m_{jet2}|\bar{\theta}_3)) + 0.5\left(P_{VV}(m_{jj}|\bar{\theta}_1)\right.$$
$$\times P_{res}(m_{jet2}|\bar{\theta}_2) P_{nonres}(m_{jet1}|\bar{\theta}_3)).$$

The resonant mass shape P_{res} is derived by fitting a dCB function to the simulated jet mass spectrum, performed separately for m_{jet1} and m_{jet2}. The resonant events are separated from the nonresonant ones when building the pdfs by requiring that there is a generated boson in a cone of $\Delta R = 0.8$ around the reconstructed merged jet. The nonresonant component of the jet mass shape is fitted separately with a Gaussian function. The contributions of W+jets and $t\bar{t}$ production are considered as one combined background shape, because both have a resonant peak around the W-boson mass, while the Z+jets background contribution is considered separately. The top mass peak does not need to be modelled since the overall contribution of $t\bar{t}$ events is less than 2%. The nonresonant dijet invariant mass shape of the V+jets backgrounds, P_{VV}, is modelled with a one dimensional kernel, in the same way as the dijet invariant mass shape of the QCD multijet background.
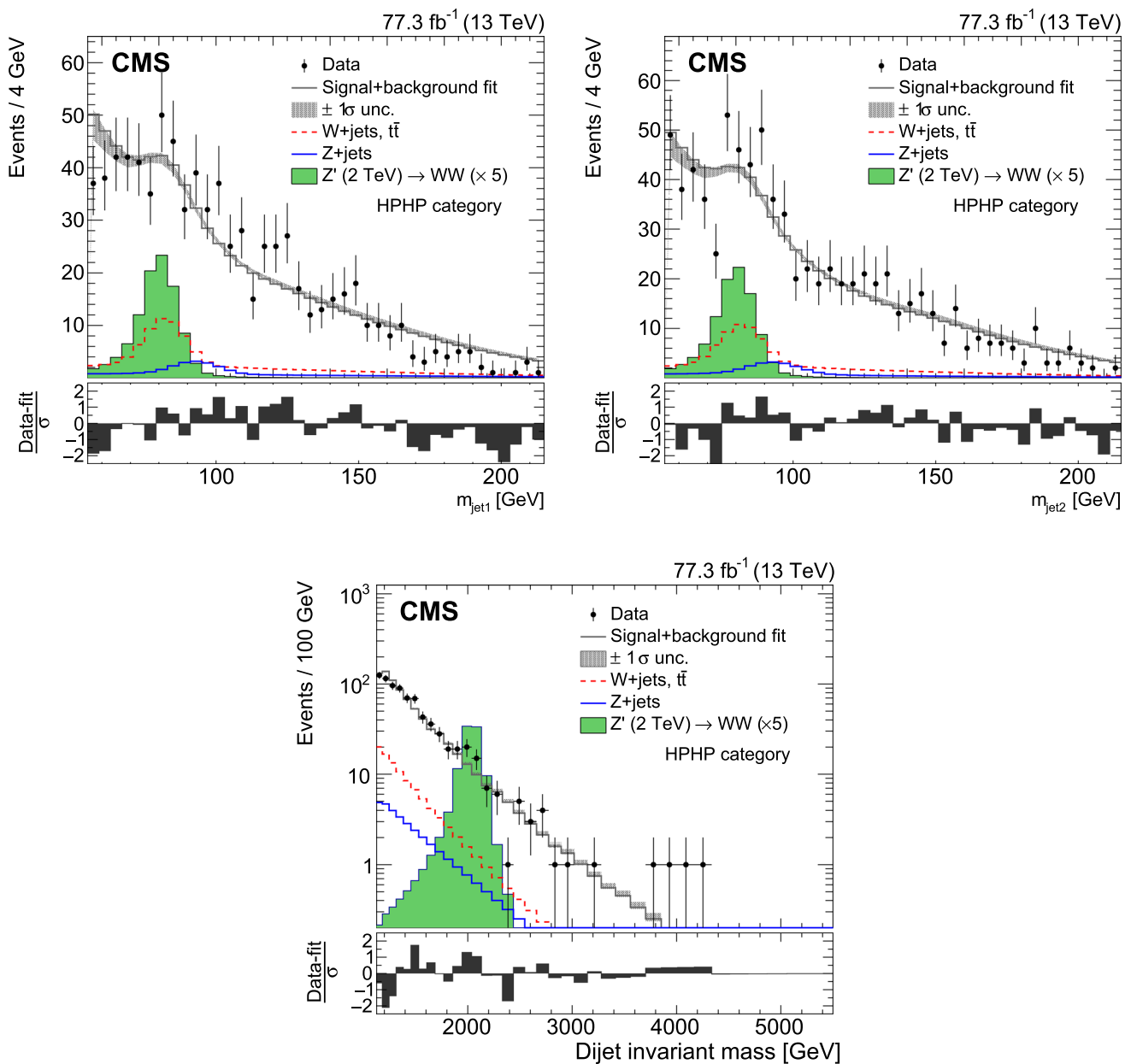
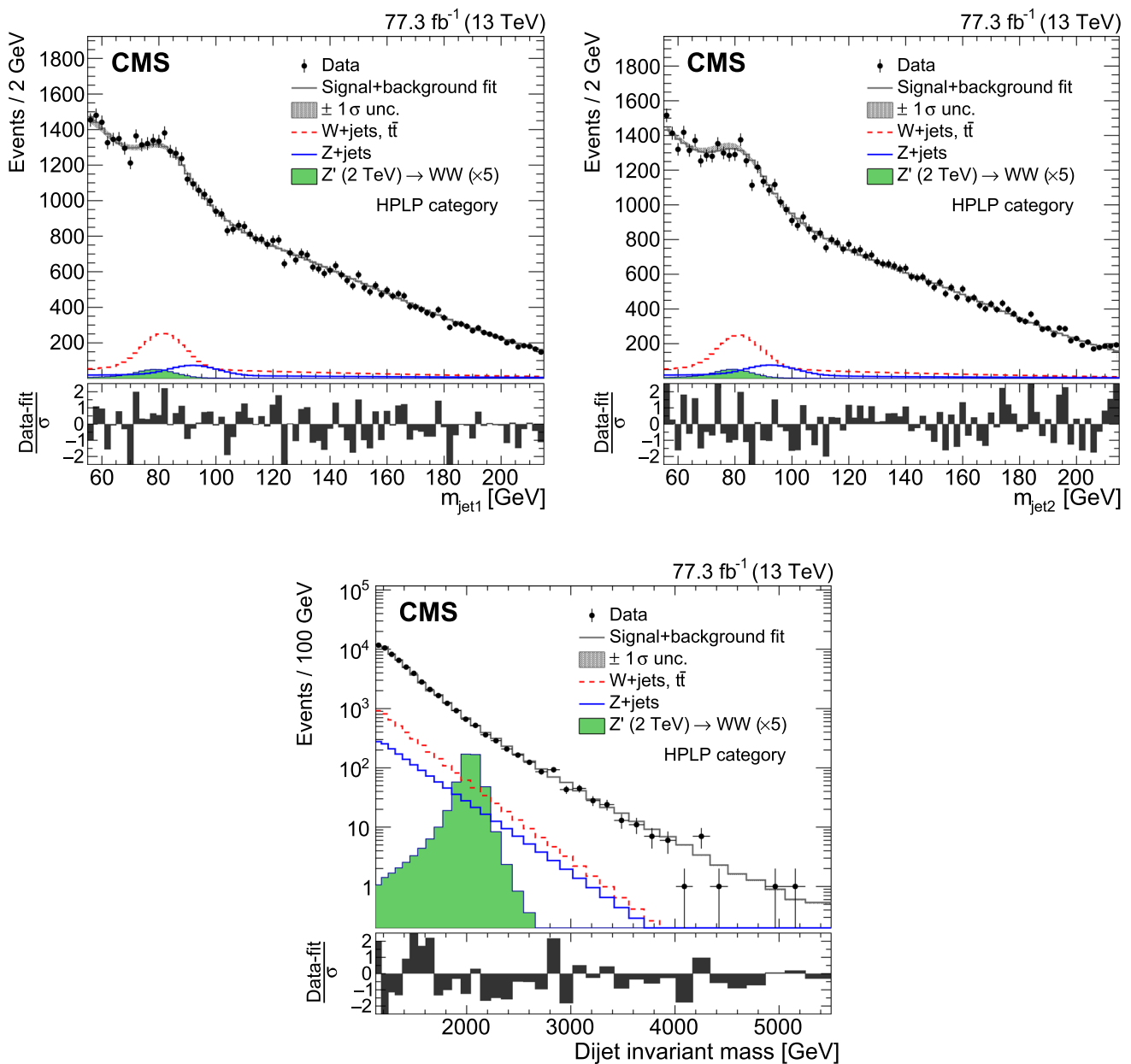**Fig. 10** For the HPHP category: comparison between the signal+background fit and the data distributions of m_{jet1} (upper left), m_{jet2} (upper right), and m_{jj} (lower). The background shape uncertainty is shown as a gray shaded band, and the statistical uncertainties of the data are shown as vertical bars. An example of a signal distribution is overlaid, where the number of expected events is scaled by a factor of 5. Shown below each mass plot is the corresponding pull distribution (Data-fit)$/\sigma$, where $\sigma = \sqrt{\sigma_{data}^2 - \sigma_{fit}^2}$ for each bin to ensure a Gaussian pull-distribution, as defined in Ref. [83]

6 Systematic uncertainties

6.1 Systematic uncertainties in the background estimation

Uncertainties in the QCD multijet background shape are included in the fit using alternative pdfs derived with the template-building method described in Sect. 5.2.1. We define five nuisance parameters that vary the shape, each of the parameters corresponding to an upward and a downward variation of alternative shapes that simultaneously affect all three dimensions. The first nuisance parameter accounts for a variation of the underlying p_T spectrum, and the two corresponding mirrored templates are obtained by applying up and down variations of the expected yields to each bin along the two jet masses and m_{jj} by a quantity proportional to m_{jet} and m_{jj}. The second nuisance parameter is a variation of

Fig. 11 For the HPLP category: comparison between the signal+background fit and the data distributions of m_{jet1} (upper left), m_{jet2} (upper right), and m_{jj} (lower). The background shape uncertainty is shown as a gray shaded band, and the statistical uncertainties of the data are shown as vertical bars. An example of a signal distribution is overlaid, where the number of expected events is scaled by a factor of 5. Shown below each mass plot is the corresponding pull distribution (Data-fit)/σ, where $\sigma = \sqrt{\sigma_{data}^2 - \sigma_{fit}^2}$ for each bin to ensure a Gaussian pull-distribution, as defined in Ref. [83]

the mass scale, and is taken into account through two mirrored alternative shapes obtained by applying up and down variations of each bin content along the two jet masses and m_{jj} by a quantity proportional to $1/m_{jet}$ and $1/m_{jj}$. Two additional alternative shapes that simultaneously affect resonance mass and jet groomed mass are also added in order to take into account differences in MC generation and modelling of the parton shower. These alternative templates are derived

using the HERWIG++ and MADGRAPH+PYTHIA8 QCD multijet simulation. This allows us to include all known background variations into the fit. For events with a large m_{jet} (> 175 GeV) and low m_{jj} (< 1200 GeV), there is an expected turn-on due to the trigger thresholds. Therefore, an additional shape uncertainty parameterizing any discrepancy between the 3D template and the QCD multijet simulation is added to the fit. Note that this shape uncertainty only affects this par-

ticular region, which is far from where a diboson signal, as relevant for this analysis, is expected. The nuisance parameters associated with these alternative shapes are constrained using Gaussian pdfs in the fit, with the pre-fit values chosen in order to cover any differences between data and simulation observed in the control regions. The alternative shapes described above are shown in Fig. 9.

A similar procedure is used for the V+jets background, adding two alternative shapes to the m_{jj} templates derived by a variation proportional to m_{jj} and $1/m_{jj}$. The resonant jet mass shapes for this background are subject to the same uncertainties as the signal. The normalizations of the V+jets and QCD background are obtained directly from simulation and are allowed to vary within 20 and 50%, respectively. The same nuisance parameters are used for the fit to 2016 and 2017 data, which reduces the fit complexity while not impacting the result of the fit.

6.2 Systematic uncertainties in the signal prediction

The dominant uncertainty in the signal selection efficiency arises from uncertainties in the boson tagging efficiency. The effect of this uncertainty is evaluated per jet and assumed to be fully correlated between both jets in the event. The W boson tagging efficiency scale factor is fully anticorrelated between the HPHP and HPLP categories (3–10%), and fully correlated between signal and V+jets backgrounds. The p_T-dependence uncertainty in the scale factor arises from the extrapolation to higher p_T's of the W boson tagging efficiency scale factors, which are measured in $t\bar{t}$ events where the jet has a p_T around 200 GeV. This uncertainty is estimated in signal simulation, and is based on the difference in tagging efficiency between the samples matched and showered either with PYTHIA or with HERWIG++, as a function of p_T, relative to the difference at 200 GeV. This is considered as correlated between the τ_{21}^{DDT} categories, and is given as $6\,(7)\%\,\ln(p_T/300\,(\text{GeV}))$ for the HPHP (HPLP) categories. The shape uncertainties in the jet masses are considered fully correlated between signal and V+jets backgrounds, allowing the data to constrain these parameters. These affect the mean and the width of the signal and V+jets pdfs. All uncertainties entering the fit are listed in Table 2.

7 Statistical interpretation

To test for the presence of narrow resonances decaying to two vector bosons we follow the CL_s prescription, evaluated using asymptotic expressions described in Refs. [80–82]. The limits are computed using a shape analysis of the three dimensional m_{jj}–m_{jet1}–m_{jet2} spectrum, where the 3D signal and background pdfs obtained above are fitted simultaneously to the data for each signal mass hypothesis and category. The

Table 3 Observed yield and background yields extracted from the background-only fit together with post-fit uncertainties, in the two purity categories

Category	HPHP	HPLP
W+jets	100 ± 11	4600 ± 200
Z+jets	33 ± 4	1580 ± 160
QCD multijets	650 ± 4	51100 ± 300
Predicted total background	783 ± 12	57200 ± 400
Observed yield	780 ± 30	57230 ± 240

signal and background yields are determined simultaneously in this fit. Systematic uncertainties are treated as nuisance parameters and profiled in the statistical interpretation using log-normal constraints, while Gaussian constraints are used for shape uncertainties.

Figures 10 and 11 show the m_{jet} and m_{jj} spectra in data for the high- and low-purity categories, respectively. The solid gray curves represent the results of the maximum likelihood fit to the data, allowing the signal yields to assume their best fit value, while the lower panels show the corresponding pull distributions, quantifying the agreement between the hypothesis of signal plus background and the data. The resonant background components are shown separately. A signal is superimposed onto all three projections corresponding to a signal yield as expected from the theoretical prediction and the analysis selection efficiency, and scaled by a factor of 5. The background yields in the signal region extracted from a background-only fit, together with their post-fit uncertainties, are summarised in Table 3 and compared with observations, separately for the two categories. The extracted V+jets cross sections are found to be compatible with the SM expectations within one standard deviation of the post-fit uncertainties.

No significant excess over the background estimation is observed. Upper limits on the production cross section at 95% confidence level (CL) are set. Limits are set in the context of the bulk graviton model and the HVT model B scenario, using the narrow-width approximation. Figure 12 shows the resulting limits as a function of the resonance mass compared to theoretical predictions. The theoretical cross sections shown in Figure 12 are calculated to LO in QCD as detailed in Refs. [6,34]. For the HVT model B, we exclude at 95% CL W' and Z' spin-1 resonances with masses below 3.8 and 3.5 TeV, respectively. In the narrow-width bulk graviton model, upper limits on the production cross sections for $G_{bulk} \rightarrow WW(ZZ)$ are set in the range from 20 (27) fb for a resonance mass of 1.2 TeV, down to 0.2 fb for a resonance mass of 5.2 TeV.

The expected upper limits obtained using the multidimensional fit method introduced here are compared to those obtained in a previous search [29] using the same data set in order to estimate the sensitivity gain by using the new
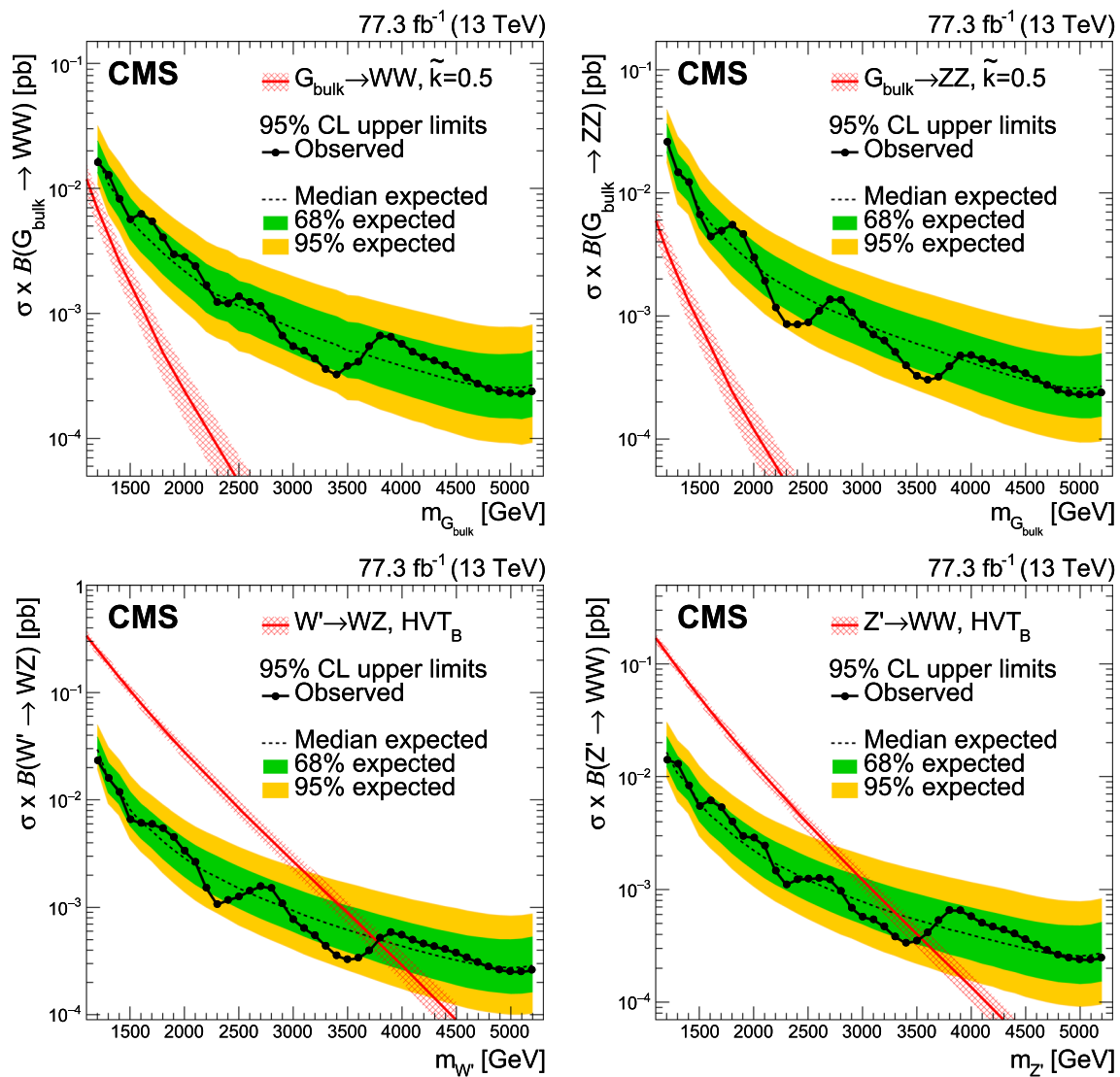
Fig. 12 Observed and expected 95% CL upper limits on the product of the production cross section (σ) and the branching fraction, obtained after combining categories of all purities with 77.3 fb^{-1} of 13 TeV data, for $G_{bulk} \rightarrow WW$ (upper left), $G_{bulk} \rightarrow ZZ$ (upper right), $W' \rightarrow WZ$ (lower left), and $Z' \rightarrow WW$ (lower right) signals. For each signal scenario the theoretical prediction (red line) and its uncertainty associated with the choice of PDF set (red hashed band) is shown. The theory cross sections (red line) are calculated at LO in QCD [6,34]

method. Figure 13 shows the expected limits for one signal model based on an analyses of the data collected in 2016, using either the fit method presented here, or previous methods. We obtain a 20–30% improvement in sensitivity when using the multi-dimensional fit method, and about a 35–40% improvement when combining the data sets recorded in 2016 and 2017 relative to the individual results. The same conclusion holds for the other signal models investigated in this paper. The results obtained with the multi-dimensional fit are the best to date in the VV channel and reach a similar sensitivity at high masses (m_X) as the combination of diboson and leptonic decay channels for the 36 fb^{-1} recorded in 2016 [27,28].

8 Summary

A search is presented for resonances with masses above 1.2 TeV that decay to WW, ZZ, or WZ boson pairs. Each of the two bosons decays into one large-radius jet, yielding dijet final states. The search is conducted using a novel approach based on a three-dimensional maximum likelihood fit in the dijet invariant mass as well as the two jet masses, thus taking advantage of the fact that the expected signal is resonant in all three mass dimensions. This method yields an improvement in sensitivity of up to 30% relative to previous search methods. The new method places additional constraints on systematic uncertainties affecting the signal by measuring
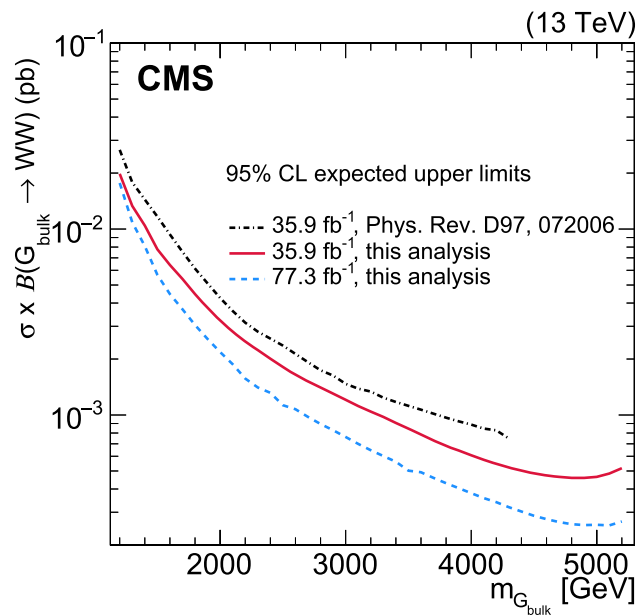
Fig. 13 Expected 95% CL upper limits on the product of the production cross section (σ) and the branching fraction for a $G_{bulk} \rightarrow WW$ signal using 35.9 fb^{-1} of data collected in 2016 obtained using the multidimensional fit method presented here (red solid line), compared to the result obtained with previous methods (black dash-dotted line) [29]. The final limit obtained when combining data collected in 2016 and 2017 is also shown (blue dashed line)

the standard model background from W or Z production with associated jets, accounting for 5% of the overall improvement in sensitivity. Decays of W and Z bosons are identified using jet substructure observables that reduce the background from quantum chromodynamics multijet production. No evidence is found for a signal, and upper limits on the resonance production cross section are set as a function of the resonance mass. The limits presented in this paper are the best to date in the dijet final state, and have a similar sensitivity as the combinations of diboson and leptonic decay channels using the 2016 data set. The results are interpreted within bulk graviton models, and as limits on the production of the W' and Z' bosons within the heavy vector triplet framework. For the heavy vector triplet model B, we exclude at 95% confidence level W' and Z' spin-1 resonances with masses below 3.8 and 3.5 TeV, respectively. In the narrow-width bulk graviton model, upper limits on the production cross sections for $G_{bulk} \rightarrow WW$ (ZZ) are set in the range of 20 (27) fb to 0.2 fb for resonance masses between 1.2 and 5.2 TeV.

References

1. L. Randall, R. Sundrum, A large mass hierarchy from a small extra dimension. Phys. Rev. Lett. **83**, 3370 (1999). https://doi.org/10.1103/PhysRevLett.83.3370. arXiv:hep-ph/9905221

2. L. Randall, R. Sundrum, An alternative to compactification. Phys. Rev. Lett. **83**, 4690 (1999). https://doi.org/10.1103/PhysRevLett.83.4690. arXiv:hep-th/9906064

3. K. Agashe, H. Davoudiasl, G. Perez, A. Soni, Warped gravitons at the LHC and beyond. Phys. Rev. D **76**, 036006 (2007). https://doi.org/10.1103/PhysRevD.76.036006. arXiv:hep-ph/0701186

4. A.L. Fitzpatrick, J. Kaplan, L. Randall, L.-T. Wang, Searching for the Kaluza–Klein graviton in bulk RS models. JHEP **09**, 013 (2007). https://doi.org/10.1088/1126-6708/2007/09/013. arXiv:hep-ph/0701150

5. O. Antipin, D. Atwood, A. Soni, Search for RS gravitons via $W_L W_L$ decays. Phys. Lett. B **666**, 155 (2008). https://doi.org/10.1016/j.physletb.2008.07.009. arXiv:0711.3175

6. D. Pappadopulo, A. Thamm, R. Torre, A. Wulzer, Heavy vector triplets: bridging theory and data. JHEP **09**, 060 (2014). https://doi.org/10.1007/JHEP09(2014)060. arXiv:1402.4431

7. CMS Collaboration, Search for massive resonances in dijet systems containing jets tagged as W or Z boson decays in pp collisions at $\sqrt{s} = 8$ TeV. JHEP **08**, 173 (2014). https://doi.org/10.1007/JHEP08(2014)173. arXiv:1405.1994

8. CMS Collaboration, Search for massive resonances decaying into pairs of boosted bosons in semi-leptonic final states at $\sqrt{s} = 8$ TeV. JHEP **08**, 174 (2014). https://doi.org/10.1007/JHEP08(2014)174. arXiv:1405.3447

9. CMS Collaboration, Search for new resonances decaying via WZ to leptons in proton-proton collisions at $\sqrt{s} = 8$ TeV. Phys. Lett. B **740**, 83 (2015). https://doi.org/10.1016/j.physletb.2014.11.026. arXiv:1407.3476

10. CMS Collaboration, Search for massive resonances decaying into WW, WZ or ZZ bosons in proton–proton collisions at $\sqrt{s} = 13$ TeV. JHEP **03**, 162 (2017). https://doi.org/10.1007/JHEP03(2017)162, arXiv:1612.09159

11. CMS Collaboration, Search for a heavy resonance decaying to a pair of vector bosons in the lepton plus merged jet final state at $\sqrt{s} = 13$ TeV. JHEP **05**, 088 (2018). https://doi.org/10.1007/JHEP05(2018)088, arXiv:1802.09407

12. CMS Collaboration, Search for narrow high-mass resonances in proton-proton collisions at $\sqrt{s} = 8$ TeV decaying to a Z and a Higgs boson. Phys. Lett. B **748**, 255 (2015). https://doi.org/10.1016/j.physletb.2015.07.011, arXiv:1502.04994

13. CMS Collaboration, Search for heavy resonances that decay into a vector boson and a Higgs boson in hadronic final states at $\sqrt{s} = 13$ TeV. Eur. Phys. J. C **77**, 636 (2017). https://doi.org/10.1140/epjc/s10052-017-5192-z, arXiv:1707.01303

14. CMS Collaboration, Search for heavy resonances decaying into a vector boson and a Higgs boson in final states with charged leptons, neutrinos, and b quarks. Phys. Lett. B **768**, 137 (2017). https://doi.org/10.1016/j.physletb.2017.02.040. arXiv:1610.08066

15. CMS Collaboration, Search for a massive resonance decaying into a Higgs boson and a W or Z boson in hadronic final states in proton-proton collisions at $\sqrt{s} = 8$ TeV. JHEP **02**, 145 (2016). https://doi.org/10.1007/JHEP02(2016)145. arXiv:1506.01443

16. CMS Collaboration, Search for massive WH resonances decaying into the $\ell\nu b\bar{b}$ final state at $\sqrt{s} = 8$ TeV. Eur. Phys. J. C **76**, 237 (2016). https://doi.org/10.1140/epjc/s10052-016-4067-z. arXiv:1601.06431

17. CMS Collaboration, Search for heavy resonances decaying to two Higgs bosons in final states containing four b quarks. Eur. Phys. J. C **76**, 371 (2016). https://doi.org/10.1140/epjc/s10052-016-4206-6. arXiv:1602.08762

18. ATLAS Collaboration, Search for WZ resonances in the fully leptonic channel using pp collisions at $\sqrt{s} = 8$ TeV collisions with the ATLAS detector. Phys. Lett. B **737**, 223 (2014). https://doi.org/10.1016/j.physletb.2014.08.039. arXiv:1406.4456

19. ATLAS Collaboration, Search for resonant diboson production in the $\ell\ell q\bar{q}$ final state in pp collisions at $\sqrt{s} = 8$ TeV with the ATLAS detector. Eur. Phys. J. C **75**, 69, (2015). https://doi.org/10.1140/epjc/s10052-015-3261-8. arXiv:1409.6190

20. ATLAS Collaboration, Search for production of WW/WZ resonances decaying to a lepton, neutrino and jets in pp collisions at $\sqrt{s} = 8$ TeV with the ATLAS detector. Eur. Phys. J. C **75**, 209, (2015). https://doi.org/10.1140/epjc/s10052-015-3425-6. arXiv:1503.04677

21. ATLAS Collaboration, Search for high-mass diboson resonances with boson-tagged jets in proton-proton collisions at $\sqrt{s} = 8$ TeV with the ATLAS detector. JHEP **12**, 055 (2015). https://doi.org/10.1007/JHEP12(2015)055. arXiv:1506.00962

22. ATLAS Collaboration, Searches for heavy diboson resonances in pp collisions at $\sqrt{s} = 13$ TeV with the ATLAS detector. JHEP **09**, 173 (2016). https://doi.org/10.1007/JHEP09(2016)173. arXiv:1606.04833

23. ATLAS Collaboration, Search for diboson resonances with boson-tagged jets in pp collisions at $\sqrt{s} = 13$ TeV with the ATLAS detector. Phys. Lett. B **777**, 91 (2018). https://doi.org/10.1016/j.physletb.2017.12.011. arXiv:1708.04445

24. ATLAS Collaboration, Search for a new resonance decaying to a W or Z boson and a Higgs boson in the $\ell\ell/\ell\nu/\nu\nu + b\bar{b}$ final states with the ATLAS detector. Eur. Phys. J. C **75**, 263 (2015). https://doi.org/10.1140/epjc/s10052-015-3474-x. arXiv:1503.08089

25. ATLAS Collaboration, Search for heavy resonances decaying to a W or Z boson and a Higgs boson in the $q\bar{q}^{(')}b\bar{b}$ final state in pp collisions at $\sqrt{s} = 13$ TeV with the ATLAS detector. Phys. Lett. B **774**, 494 (2017). https://doi.org/10.1016/j.physletb.2017.09.066. arXiv:1707.06958

26. ATLAS Collaboration, Search for new resonances decaying to a W or Z boson and a Higgs boson in the $\ell^+\ell^- b\bar{b}$, $\ell\nu b\bar{b}$, and $\nu\bar{\nu} b\bar{b}$ channels with pp collisions at $\sqrt{s} = 13$ TeV with the ATLAS detector. Phys. Lett. B **765**, 32 (2017). https://doi.org/10.1016/j.physletb.2016.11.045. arXiv:1607.05621

27. CMS Collaboration, Combination of CMS searches for heavy resonances decaying to pairs of bosons or leptons (2019). arXiv:1906.00057

28. ATLAS Collaboration, Combination of searches for heavy resonances decaying into bosonic and leptonic final states using 36 fb^{-1} of proton-proton collision data at $\sqrt{s} = 13\,TeV$ with the ATLAS detector. Phys. Rev. D **052008** (2018). https://doi.org/10.1103/PhysRevD.98.052008. arXiv:1808.02380

29. CMS Collaboration, Search for massive resonances decaying into WW, WZ, ZZ, qW, and qZ with dijet final states at $\sqrt{s} = 13$ TeV. Phys. Rev. D **97**, 072006 (2018). https://doi.org/10.1103/PhysRevD.97.072006. arXiv:1708.05379

30. CMS Collaboration, The CMS experiment at the CERN LHC. JINST **3**, S08004 (2008). https://doi.org/10.1088/1748-0221/3/08/S08004

31. CMS Collaboration, The CMS trigger system. JINST **12**, P01020 (2017). https://doi.org/10.1088/1748-0221/12/01/P01020. arXiv:1609.02366

32. C. Grojean, E. Salvioni, R. Torre, A weakly constrained W' at the early LHC. JHEP **07**, 002 (2011). https://doi.org/10.1007/JHEP07(2011)002. arXiv:1103.2761

33. E. Salvioni, G. Villadoro, F. Zwirner, Minimal Z' models: present bounds and early LHC reach. JHEP **11**, 068 (2009). https://doi.org/10.1088/1126-6708/2009/11/068. arXiv:0909.1320

34. A. Oliveira, Gravity particles from warped extra dimensions. Predict. LHC (2014). arXiv:1404.0102

35. B. Bellazzini, C. Csáki, J. Serra, Composite Higgses. Eur. Phys. J. C **74**, 2766 (2014). https://doi.org/10.1140/epjc/s10052-014-2766-x. arXiv:1401.2457

36. R. Contino, D. Marzocca, D. Pappadopulo, R. Rattazzi, On the effect of resonances in composite Higgs phenomenology. JHEP **10**, 081 (2011). https://doi.org/10.1007/JHEP10(2011)081. arXiv:1109.1570

37. D. Marzocca, M. Serone, J. Shu, General composite Higgs models. JHEP **08**, 013 (2012). https://doi.org/10.1007/JHEP08(2012)013. arXiv:1205.0770

38. D. Greco, D. Liu, Hunting composite vector resonances at the LHC: naturalness facing data. JHEP **12**, 126 (2014). https://doi.org/10.1007/JHEP12(2014)126. arXiv:1410.2883

39. K. Lane, L. Pritchett, The light composite Higgs boson in strong extended technicolor. JHEP **06**, 140 (2017). https://doi.org/10.1007/JHEP06(2017)140. arXiv:1604.07085

40. M. Schmaltz, D. Tucker-Smith, Little Higgs review. Ann. Rev. Nucl. Part. Sci. **55**, 229 (2005). https://doi.org/10.1146/annurev.nucl.55.090704.151502. arXiv:hep-ph/0502182

41. N. Arkani-Hamed, A.G. Cohen, E. Katz, A.E. Nelson, The littlest Higgs. JHEP **07**, 034 (2002). https://doi.org/10.1088/1126-6708/2002/07/034. arXiv:hep-ph/0206021

42. J. Alwall et al., The automated computation of tree-level and next-to-leading order differential cross sections, and their matching to parton shower simulations. JHEP **07**, 079 (2014). https://doi.org/10.1007/JHEP07(2014)079. arXiv:1405.0301

43. T. Sjöstrand et al., An introduction to PYTHIA 8.2. Comput. Phys. Commun. **191**, 159 (2015). https://doi.org/10.1016/j.cpc.2015.01.024. arXiv:1410.3012

44. NNPDF Collaboration, Parton distributions for the LHC Run II. JHEP **04**, 040 (2015). https://doi.org/10.1007/JHEP04(2015)040. arXiv:1410.8849

45. CMS Collaboration, Event generator tunes obtained from underlying event and multiparton scattering measurements. Eur. Phys. J. C **76**, 155 (2016). https://doi.org/10.1140/epjc/s10052-016-3988-x. arXiv:1512.00815

46. CMS Collaboration, Extraction and validation of a new set of CMS PYTHIA8 tunes from underlying-event measurements (2019). arXiv:1903.12179. Submitted to Eur. Phys. J. C

47. J. Alwall et al., Comparative study of various algorithms for the merging of parton showers and matrix elements in hadronic collisions. Eur. Phys. J. C **53**, 473 (2008). https://doi.org/10.1140/epjc/s10052-007-0490-5. arXiv:0706.2569

48. S. Alioli et al., Jet pair production in POWHEG. JHEP **04**, 081 (2011). https://doi.org/10.1007/JHEP04(2011)081. arXiv:1012.3380

49. P. Nason, A new method for combining NLO QCD with shower Monte Carlo algorithms. JHEP **11**, 040 (2004). https://doi.org/10.1088/1126-6708/2004/11/040. arXiv:hep-ph/0409146

50. S. Frixione, P. Nason, C. Oleari, Matching NLO QCD computations with parton shower simulations: the POWHEG method. JHEP **11**, 070 (2007). https://doi.org/10.1088/1126-6708/2007/11/070. arXiv:0709.2092

51. S. Alioli, P. Nason, C. Oleari, E. Re, A general framework for implementing NLO calculations in shower Monte Carlo programs: the POWHEG BOX. JHEP **06**, 043 (2010). https://doi.org/10.1007/JHEP06(2010)043. arXiv:1002.2581

52. M. Bähr et al., Herwig++ physics and manual. Eur. Phys. J. C **58**, 639 (2008). https://doi.org/10.1140/epjc/s10052-008-0798-9. arXiv:0803.0883

53. S. Alioli, S.-O. Moch, P. Uwer, Hadronic top-quark pair-production with one jet and parton showering. JHEP **01**, 137 (2012). https://doi.org/10.1007/JHEP01(2012)137. arXiv:1110.5251

54. S. Kallweit et al., NLO electroweak automation and precise predictions for W+multijet production at the LHC. JHEP **04**, 012 (2015). https://doi.org/10.1007/JHEP04(2015)012. arXiv:1412.5157

55. S. Kallweit et al., NLO QCD+EW predictions for V+jets including off-shell vector-boson decays and multijet merging. JHEP **04**, 021 (2016). https://doi.org/10.1007/JHEP04(2016)021. arXiv:1511.08692

56. NNPDF Collaboration, Parton distributions from high-precision collider data. Eur. Phys. J. C **77**, 663 (2017). https://doi.org/10.1140/epjc/s10052-017-5199-5. arXiv:1706.00428

57. GEANT4 Collaboration, Geant4—a simulation toolkit. Nucl. Instrum. Meth. A **506**, 250 (2003). https://doi.org/10.1016/S0168-9002(03)01368-8

58. CMS Collaboration, Particle-flow reconstruction and global event description with the CMS detector. JINST **12**, P10003 (2017). https://doi.org/10.1088/1748-0221/12/10/P10003. arXiv:1706.04965

59. M. Cacciari, G.P. Salam, G. Soyez, The anti-k_T jet clustering algorithm. JHEP **04**, 063 (2008). https://doi.org/10.1088/1126-6708/2008/04/063. arXiv:0802.1189

60. M. Cacciari, G.P. Salam, G. Soyez, FastJet user manual. Eur. Phys. J. C **72**, 1896 (2012). https://doi.org/10.1140/epjc/s10052-012-1896-2. arXiv:1111.6097

61. D. Bertolini, P. Harris, M. Low, N. Tran, Pileup per particle identification. JHEP **10**, 59 (2014). https://doi.org/10.1007/JHEP10(2014)059. arXiv:1407.6013

62. CMS Collaboration, Jet algorithms performance in 13 TeV data. CMS Physics Analysis Summary CMS-PAS-JME-16-003 (2016). http://cds.cern.ch/record/2256875

63. CMS Collaboration, Jet energy scale and resolution in the CMS experiment in pp collisions at 8 TeV. JINST **12**, P02014 (2017). https://doi.org/10.1088/1748-0221/12/02/P02014. arXiv:1607.03663

64. M. Cacciari, G.P. Salam, G. Soyez, The catchment area of jets. JHEP **04**, 005 (2008). https://doi.org/10.1088/1126-6708/2008/04/005. arXiv:0802.1188

65. M. Dasgupta, A. Fregoso, S. Marzani, G.P. Salam, Towards an understanding of jet substructure. JHEP **09**, 029 (2013). https://doi.org/10.1007/JHEP09(2013)029. arXiv:1307.0007

66. J.M. Butterworth, A.R. Davison, M. Rubin, G.P. Salam, Jet substructure as a new Higgs search channel at the LHC. Phys. Rev. Lett. **100**, 242001 (2008). https://doi.org/10.1103/PhysRevLett.100.242001. arXiv:0802.2470

67. A.J. Larkoski, S. Marzani, G. Soyez, J. Thaler, Soft drop. JHEP **05**, 146 (2014). https://doi.org/10.1007/JHEP05(2014)146. arXiv:1402.2657

68. J. Thaler, K. Van Tilburg, Maximizing boosted top identification by minimizing N-subjettiness. JHEP **02**, 093 (2012). https://doi.org/10.1007/JHEP02(2012)093. arXiv:1108.2701

69. Y.L. Dokshitzer, G.D. Leder, S. Moretti, B.R. Webber, Better jet clustering algorithms. JHEP **08**, 001 (1997). https://doi.org/10.1088/1126-6708/1997/08/001. arXiv:hep-ph/9707323

70. M. Wobisch, T. Wengler, Hadronization corrections to jet cross-sections in deep inelastic scattering. In: Monte Carlo generators for HERA physics (1998). arXiv:hep-ph/9907280

71. D. Krohn, J. Thaler, L.-T. Wang, Jet trimming. JHEP **02**, 084 (2010). https://doi.org/10.1007/JHEP02(2010)084. arXiv:0912.1342

72. S. Catani, YuL Dokshitzer, M.H. Seymour, B.R. Webber, Longitudinally invariant k_T clustering algorithms for hadron hadron collisions. Nucl. Phys. B **406**, 187 (1993). https://doi.org/10.1016/0550-3213(93)90166-M

73. J. Dolen et al., Thinking outside the ROCs: designing decorrelated taggers (DDT) for jet substructure. JHEP **05**, 156 (2016). https://doi.org/10.1007/JHEP05(2016)156. arXiv:1603.00027

74. CMS Collaboration, Description and performance of track and primary-vertex reconstruction with the CMS tracker. JINST **9**, P10009 (2014). https://doi.org/10.1088/1748-0221/9/10/P10009. arXiv:1405.6569

75. CMS Collaboration, Performance of the CMS muon detector and muon reconstruction with proton–proton collisions at $\sqrt{s} = 13$ TeV. JINST **13**, P06015 (2018). https://doi.org/10.1088/1748-0221/13/06/P06015. arXiv:1804.04528

76. CMS Collaboration, Performance of electron reconstruction and selection with the CMS detector in proton-proton collisions at $\sqrt{s} = 8$ TeV. JINST **10**, P06005 (2015). https://doi.org/10.1088/1748-0221/10/06/P06005. arXiv:1502.02701

77. CMS Collaboration, Measurement of differential cross sections for top quark pair production using the lepton+jets final state in proton–proton collisions at 13 TeV. Phys. Rev. D **95**, 092001 (2017). https://doi.org/10.1103/PhysRevD.95.092001. arXiv:1610.04191

78. M. Oreglia, A study of the reactions $\psi' \rightarrow \gamma\gamma\psi$. PhD thesis, SLAC, (1980)

79. K.S. Cranmer, Kernel estimation in high-energy physics. Comput. Phys. Commun. **136**, 198 (2001). https://doi.org/10.1016/S0010-4655(00)00243-5. arXiv:hep-ex/0011057

80. A.L. Read, Presentation of search results: the CL$_s$ technique. J. Phys. G **28**, 2693 (2002). https://doi.org/10.1088/0954-3899/28/10/313

81. T. Junk, Confidence level computation for combining searches with small statistics. Nucl. Instrum. Meth. A **434**, 435 (1999). https://doi.org/10.1016/S0168-9002(99)00498-2. arXiv:hep-ex/9902006

82. G. Cowan, K. Cranmer, E. Gross, O. Vitells, Asymptotic formulae for likelihood-based tests of new physics. Eur. Phys. J. C **71**, 1554 (2011). https://doi.org/10.1140/epjc/s10052-011-1554-0. arXiv:1007.1727. [Erratum: 10.1140/epjc/s10052-013-2501-z]

83. L. Demortier, L. Lyons, Everything you always wanted to know about pulls. Technical Report CDF/ANAL/PUBLIC/5776, CDF (2002)

CMS Collaboration

Yerevan Physics Institute, Yerevan, Armenia

A. M. Sirunyan[†], A. Tumasyan

Institut für Hochenergiephysik, Wien, Austria

W. Adam, F. Ambrogi, T. Bergauer, J. Brandstetter, M. Dragicevic, J. Erö, A. Escalante Del Valle, M. Flechl,
R. Frühwirth[1], M. Jeitler[1], N. Krammer, I. Krätschmer, D. Liko, T. Madlener, I. Mikulec, N. Rad, J. Schieck[1],
R. Schöfbeck, M. Spanring, D. Spitzbart, W. Waltenberger, C.-E. Wulz[1], M. Zarucki

Institute for Nuclear Problems, Minsk, Belarus

V. Drugakov, V. Mossolov, J. Suarez Gonzalez

Universiteit Antwerpen, Antwerpen, Belgium

M. R. Darwish, E. A. De Wolf, D. Di Croce, X. Janssen, J. Lauwers, A. Lelek, M. Pieters, H. Rejeb Sfar,
H. Van Haevermaet, P. Van Mechelen, S. Van Putte, N. Van Remortel

Vrije Universiteit Brussel, Brussel, Belgium

F. Blekman, E. S. Bols, S. S. Chhibra, J. D'Hondt, J. De Clercq, D. Lontkovskyi, S. Lowette, I. Marchesini, S. Moortgat,
L. Moreels, Q. Python, K. Skovpen, S. Tavernier, W. Van Doninck, P. Van Mulders, I. Van Parijs

Université Libre de Bruxelles, Bruxelles, Belgium

D. Beghin, B. Bilin, H. Brun, B. Clerbaux, G. De Lentdecker, H. Delannoy, B. Dorney, L. Favart, A. Grebenyuk,
A. K. Kalsi, J. Luetic, A. Popov, N. Postiau, E. Starling, L. Thomas, C. Vander Velde, P. Vanlaer, D. Vannerom

Ghent University, Ghent, Belgium

T. Cornelis, D. Dobur, I. Khvastunov[2], M. Niedziela, C. Roskas, D. Trocino, M. Tytgat, W. Verbeke, B. Vermassen, M. Vit,
N. Zaganidis

Université Catholique de Louvain, Louvain-la-Neuve, Belgium

O. Bondu, G. Bruno, C. Caputo, P. David, C. Delaere, M. Delcourt, A. Giammanco, V. Lemaitre, A. Magitteri,
J. Prisciandaro, A. Saggio, M. Vidal Marono, P. Vischia, J. Zobec

Centro Brasileiro de Pesquisas Fisicas, Rio de Janeiro, Brazil

F. L. Alves, G. A. Alves, G. Correia Silva, C. Hensel, A. Moraes, P. Rebello Teles

Universidade do Estado do Rio de Janeiro, Rio de Janeiro, Brazil

E. Belchior Batista Das Chagas, W. Carvalho, J. Chinellato[3], E. Coelho, E. M. Da Costa, G. G. Da Silveira[4],

D. De Jesus Damiao, C. De Oliveira Martins, S. Fonseca De Souza, L. M. Huertas Guativa, H. Malbouisson, J. Martins[5], D. Matos Figueiredo, M. Medina Jaime[6], M. Melo De Almeida, C. Mora Herrera, L. Mundim, H. Nogima, W. L. Prado Da Silva, L. J. Sanchez Rosas, A. Santoro, A. Sznajder, M. Thiel, E. J. Tonelli Manganote[3], F. Torres Da Silva De Araujo, A. Vilela Pereira

Universidade Estadual Paulista[a], Universidade Federal do ABC[b], São Paulo, Brazil
S. Ahuja[a], C. A. Bernardes[a], L. Calligaris[a], T. R. Fernandez Perez Tomei[a], E. M. Gregores[b], D. S. Lemos, P. G. Mercadante[b], S. F. Novaes[a], SandraS. Padula[a]

Institute for Nuclear Research and Nuclear Energy, Bulgarian Academy of Sciences, Sofia, Bulgaria
A. Aleksandrov, G. Antchev, R. Hadjiiska, P. Iaydjiev, A. Marinov, M. Misheva, M. Rodozov, M. Shopova, G. Sultanov

University of Sofia, Sofia, Bulgaria
M. Bonchev, A. Dimitrov, T. Ivanov, L. Litov, B. Pavlov, P. Petkov

Beihang University, Beijing, China
W. Fang[7], X. Gao[7], L. Yuan

Department of Physics, Tsinghua University, Beijing, China
Z. Hu, Y. Wang

Institute of High Energy Physics, Beijing, China
M. Ahmad, G. M. Chen[8], H. S. Chen[8], M. Chen, C. H. Jiang, D. Leggat, H. Liao, Z. Liu, S. M. Shaheen[8], A. Spiezia, J. Tao, E. Yazgan, H. Zhang, S. Zhang[8], J. Zhao

State Key Laboratory of Nuclear Physics and Technology, Peking University, Beijing, China
A. Agapitos, Y. Ban, G. Chen, A. Levin, J. Li, L. Li, Q. Li, Y. Mao, S. J. Qian, D. Wang, Q. Wang

Universidad de Los Andes, Bogota, Colombia
C. Avila, A. Cabrera, L. F. Chaparro Sierra, C. Florez, C. F. González Hernández, M. A. Segura Delgado

Universidad de Antioquia, Medellin, Colombia
J. Mejia Guisao, J. D. Ruiz Alvarez, C. A. Salazar González, N. Vanegas Arbelaez

University of Split, Faculty of Electrical Engineering, Mechanical Engineering and Naval Architecture, Split, Croatia
D. Giljanović, N. Godinovic, D. Lelas, I. Puljak, T. Sculac

University of Split, Faculty of Science, Split, Croatia
Z. Antunovic, M. Kovac

Institute Rudjer Boskovic, Zagreb, Croatia
V. Brigljevic, S. Ceci, D. Ferencek, K. Kadija, B. Mesic, M. Roguljic, A. Starodumov[9], T. Susa

University of Cyprus, Nicosia, Cyprus
M. W. Ather, A. Attikis, E. Erodotou, A. Ioannou, M. Kolosova, S. Konstantinou, G. Mavromanolakis, J. Mousa, C. Nicolaou, F. Ptochos, P. A. Razis, H. Rykaczewski, D. Tsiakkouri

Charles University, Prague, Czech Republic
M. Finger[10], M. Finger Jr.[10], A. Kveton, J. Tomsa

Escuela Politecnica Nacional, Quito, Ecuador
E. Ayala

Universidad San Francisco de Quito, Quito, Ecuador
E. Carrera Jarrin

Academy of Scientific Research and Technology of the Arab Republic of Egypt, Egyptian Network of High Energy Physics, Cairo, Egypt
S. Abu Zeid[11], S. Khalil[12]

National Institute of Chemical Physics and Biophysics, Tallinn, Estonia
S. Bhowmik, A. Carvalho Antunes De Oliveira, R. K. Dewanjee, K. Ehataht, M. Kadastik, M. Raidal, C. Veelken

Department of Physics, University of Helsinki, Helsinki, Finland

P. Eerola, L. Forthomme, H. Kirschenmann, K. Osterberg, M. Voutilainen

Helsinki Institute of Physics, Helsinki, Finland

F. Garcia, J. Havukainen, J. K. Heikkilä, T. Järvinen, V. Karimäki, R. Kinnunen, T. Lampén, K. Lassila-Perini, S. Laurila, S. Lehti, T. Lindén, P. Luukka, T. Mäenpää, H. Siikonen, E. Tuominen, J. Tuominiemi

Lappeenranta University of Technology, Lappeenranta, Finland

T. Tuuva

IRFU, CEA, Université Paris-Saclay, Gif-sur-Yvette, France

M. Besancon, F. Couderc, M. Dejardin, D. Denegri, B. Fabbro, J. L. Faure, F. Ferri, S. Ganjour, A. Givernaud, P. Gras, G. Hamel de Monchenault, P. Jarry, C. Leloup, E. Locci, J. Malcles, J. Rander, A. Rosowsky, M. Ö. Sahin, A. Savoy-Navarro[13], M. Titov

Laboratoire Leprince-Ringuet, CNRS/IN2P3, Ecole Polytechnique, Institut Polytechnique de Paris, Paris, France

C. Amendola, F. Beaudette, P. Busson, C. Charlot, B. Diab, G. Falmagne, R. Granier de Cassagnac, I. Kucher, A. Lobanov, C. Martin Perez, M. Nguyen, C. Ochando, P. Paganini, J. Rembser, R. Salerno, J. B. Sauvan, Y. Sirois, A. Zabi, A. Zghiche

Université de Strasbourg, CNRS, IPHC UMR 7178, Strasbourg, France

J.-L. Agram[14], J. Andrea, D. Bloch, G. Bourgatte, J.-M. Brom, E. C. Chabert, C. Collard, E. Conte[14], J.-C. Fontaine[14], D. Gelé, U. Goerlach, M. Jansová, A.-C. Le Bihan, N. Tonon, P. Van Hove

Centre de Calcul de l'Institut National de Physique Nucleaire et de Physique des Particules, CNRS/IN2P3, Villeurbanne, France

S. Gadrat

Université de Lyon, Université Claude Bernard Lyon 1, CNRS-IN2P3, Institut de Physique Nucléaire de Lyon, Villeurbanne, France

S. Beauceron, C. Bernet, G. Boudoul, C. Camen, N. Chanon, R. Chierici, D. Contardo, P. Depasse, H. El Mamouni, J. Fay, S. Gascon, M. Gouzevitch, B. Ille, Sa. Jain, F. Lagarde, I. B. Laktineh, H. Lattaud, M. Lethuillier, L. Mirabito, S. Perries, V. Sordini, G. Touquet, M. Vander Donckt, S. Viret

Georgian Technical University, Tbilisi, Georgia

G. Adamov

Tbilisi State University, Tbilisi, Georgia

Z. Tsamalaidze[10]

RWTH Aachen University, I. Physikalisches Institut, Aachen, Germany

C. Autermann, L. Feld, M. K. Kiesel, K. Klein, M. Lipinski, D. Meuser, A. Pauls, M. Preuten, M. P. Rauch, C. Schomakers, J. Schulz, M. Teroerde, B. Wittmer

RWTH Aachen University, III. Physikalisches Institut A, Aachen, Germany

A. Albert, M. Erdmann, S. Erdweg, T. Esch, B. Fischer, R. Fischer, S. Ghosh, T. Hebbeker, K. Hoepfner, H. Keller, L. Mastrolorenzo, M. Merschmeyer, A. Meyer, P. Millet, G. Mocellin, S. Mondal, S. Mukherjee, D. Noll, A. Novak, T. Pook, A. Pozdnyakov, T. Quast, M. Radziej, Y. Rath, H. Reithler, M. Rieger, J. Roemer, A. Schmidt, S. C. Schuler, A. Sharma, S. Thüer, S. Wiedenbeck

RWTH Aachen University, III. Physikalisches Institut B, Aachen, Germany

G. Flügge, W. Haj Ahmad[15], O. Hlushchenko, T. Kress, T. Müller, A. Nehrkorn, A. Nowack, C. Pistone, O. Pooth, D. Roy, H. Sert, A. Stahl[16]

Deutsches Elektronen-Synchrotron, Hamburg, Germany

M. Aldaya Martin, P. Asmuss, I. Babounikau, H. Bakhshiansohi, K. Beernaert, O. Behnke, U. Behrens, A. Bermúdez Martínez, D. Bertsche, A. A. Bin Anuar, K. Borras[17], V. Botta, A. Campbell, A. Cardini, P. Connor, S. Consuegra Rodríguez, C. Contreras-Campana, V. Danilov, A. De Wit, M. M. Defranchis, C. Diez Pardos, D. Domínguez Damiani, G. Eckerlin, D. Eckstein, T. Eichhorn, A. Elwood, E. Eren, E. Gallo[18], A. Geiser, J. M. Grados Luyando, A. Grohsjean, M. Guthoff, M. Haranko, A. Harb, A. Jafari, N. Z. Jomhari, H. Jung, A. Kasem[17],

M. Kasemann, H. Kaveh, J. Keaveney, C. Kleinwort, J. Knolle, D. Krücker, W. Lange, T. Lenz, J. Leonard, J. Lidrych, K. Lipka, W. Lohmann[19], R. Mankel, I.-A. Melzer-Pellmann, A. B. Meyer, M. Meyer, M. Missiroli, G. Mittag, J. Mnich, A. Mussgiller, V. Myronenko, D. Pérez Adán, S. K. Pflitsch, D. Pitzl, A. Raspereza, A. Saibel, M. Savitskyi, V. Scheurer, P. Schütze, C. Schwanenberger, R. Shevchenko, A. Singh, H. Tholen, O. Turkot, A. Vagnerini, M. Van De Klundert, G. P. Van Onsem, R. Walsh, Y. Wen, K. Wichmann, C. Wissing, O. Zenaiev, R. Zlebcik

University of Hamburg, Hamburg, Germany
R. Aggleton, S. Bein, L. Benato, A. Benecke, V. Blobel, T. Dreyer, A. Ebrahimi, A. Fröhlich, C. Garbers, E. Garutti, D. Gonzalez, P. Gunnellini, J. Haller, A. Hinzmann, A. Karavdina, G. Kasieczka, R. Klanner, R. Kogler, N. Kovalchuk, S. Kurz, V. Kutzner, J. Lange, T. Lange, A. Malara, D. Marconi, J. Multhaup, C. E. N. Niemeyer, D. Nowatschin, A. Perieanu, A. Reimers, O. Rieger, C. Scharf, P. Schleper, S. Schumann, J. Schwandt, J. Sonneveld, H. Stadie, G. Steinbrück, F. M. Stober, M. Stöver, B. Vormwald, I. Zoi

Karlsruher Institut fuer Technologie, Karlsruhe, Germany
C. Barth, M. Baselga, S. Baur, T. Berger, E. Butz, R. Caspart, T. Chwalek, W. De Boer, A. Dierlamm, K. El Morabit, N. Faltermann, M. Giffels, P. Goldenzweig, A. Gottmann, M. A. Harrendorf, F. Hartmann[16], U. Husemann, S. Kudella, S. Mitra, M. U. Mozer, Th. Müller, M. Musich, A. Nürnberg, G. Quast, K. Rabbertz, D. Schäfer, M. Schröder, I. Shvetsov, H. J. Simonis, R. Ulrich, M. Weber, C. Wöhrmann, R. Wolf

Institute of Nuclear and Particle Physics (INPP), NCSR Demokritos, Aghia Paraskevi, Greece
G. Anagnostou, P. Asenov, G. Daskalakis, T. Geralis, A. Kyriakis, D. Loukas, G. Paspalaki

National and Kapodistrian University of Athens, Athens, Greece
M. Diamantopoulou, G. Karathanasis, P. Kontaxakis, A. Panagiotou, I. Papavergou, N. Saoulidou, A. Stakia, K. Theofilatos, K. Vellidis

National Technical University of Athens, Athens, Greece
G. Bakas, K. Kousouris, I. Papakrivopoulos, G. Tsipolitis

University of Ioánnina, Ioánnina, Greece
I. Evangelou, C. Foudas, P. Gianneios, P. Katsoulis, P. Kokkas, S. Mallios, K. Manitara, N. Manthos, I. Papadopoulos, J. Strologas, F. A. Triantis, D. Tsitsonis

MTA-ELTE Lendület CMS Particle and Nuclear Physics Group, Eötvös Loránd University, Budapest, Hungary
M. Bartók[20], M. Csanad, P. Major, K. Mandal, A. Mehta, M. I. Nagy, G. Pasztor, O. Surányi, G. I. Veres

Wigner Research Centre for Physics, Budapest, Hungary
G. Bencze, C. Hajdu, D. Horvath[21], F. Sikler, T. Á. Vámi, V. Veszpremi, G. Vesztergombi[†]

Institute of Nuclear Research ATOMKI, Debrecen, Hungary
N. Beni, S. Czellar, J. Karancsi[20], A. Makovec, J. Molnar, Z. Szillasi

Institute of Physics, University of Debrecen, Debrecen, Hungary
P. Raics, D. Teyssier, Z. L. Trocsanyi, B. Ujvari

Eszterhazy Karoly University, Karoly Robert Campus, Gyongyos, Hungary
T. Csorgo, W. J. Metzger, F. Nemes, T. Novak

Indian Institute of Science (IISc), Bangalore, India
S. Choudhury, J. R. Komaragiri, P. C. Tiwari

National Institute of Science Education and Research, HBNI, Bhubaneswar, India
S. Bahinipati[23], C. Kar, G. Kole, P. Mal, V. K. Muraleedharan Nair Bindhu, A. Nayak[24], D. K. Sahoo[23], S. K. Swain

Panjab University, Chandigarh, India
S. Bansal, S. B. Beri, V. Bhatnagar, S. Chauhan, R. Chawla, N. Dhingra, R. Gupta, A. Kaur, M. Kaur, S. Kaur, P. Kumari, M. Lohan, M. Meena, K. Sandeep, S. Sharma, J. B. Singh, A. K. Virdi, G. Walia

University of Delhi, Delhi, India

A. Bhardwaj, B. C. Choudhary, R. B. Garg, M. Gola, S. Keshri, Ashok Kumar, S. Malhotra, M. Naimuddin, P. Priyanka, K. Ranjan, Aashaq Shah, R. Sharma

Saha Institute of Nuclear Physics, HBNI, Kolkata, India

R. Bhardwaj[25], M. Bharti[25], R. Bhattacharya, S. Bhattacharya, U. Bhawandeep[25], D. Bhowmik, S. Dey, S. Dutta, S. Ghosh, M. Maity[26], K. Mondal, S. Nandan, A. Purohit, P. K. Rout, G. Saha, S. Sarkar, T. Sarkar[26], M. Sharan, B. Singh[25], S. Thakur[25]

Indian Institute of Technology Madras, Chennai, India

P. K. Behera, P. Kalbhor, A. Muhammad, P. R. Pujahari, A. Sharma, A. K. Sikdar

Bhabha Atomic Research Centre, Mumbai, India

R. Chudasama, D. Dutta, V. Jha, V. Kumar, D. K. Mishra, P. K. Netrakanti, L. M. Pant, P. Shukla

Tata Institute of Fundamental Research-A, Mumbai, India

T. Aziz, M. A. Bhat, S. Dugad, G. B. Mohanty, N. Sur, RavindraKumar Verma

Tata Institute of Fundamental Research-B, Mumbai, India

S. Banerjee, S. Bhattacharya, S. Chatterjee, P. Das, M. Guchait, S. Karmakar, S. Kumar, G. Majumder, K. Mazumdar, N. Sahoo, S. Sawant

Indian Institute of Science Education and Research (IISER), Pune, India

S. Chauhan, S. Dube, V. Hegde, A. Kapoor, K. Kothekar, S. Pandey, A. Rane, A. Rastogi, S. Sharma

Institute for Research in Fundamental Sciences (IPM), Tehran, Iran

S. Chenarani[27], E. Eskandari Tadavani, S. M. Etesami[27], M. Khakzad, M. Mohammadi Najafabadi, M. Naseri, F. Rezaei Hosseinabadi

University College Dublin, Dublin, Ireland

M. Felcini, M. Grunewald

INFN Sezione di Bari[a], Università di Bari[b], Politecnico di Bari[c], Bari, Italy

M. Abbrescia[a,b], R. Aly[a,b,28], C. Calabria[a,b], A. Colaleo[a], D. Creanza[a,c], L. Cristella[a,b], N. De Filippis[a,c], M. De Palma[a,b], A. Di Florio[a,b], L. Fiore[a], A. Gelmi[a,b], G. Iaselli[a,c], M. Ince[a,b], S. Lezki[a,b], G. Maggi[a,c], M. Maggi[a], G. Miniello[a,b], S. My[a,b], S. Nuzzo[a,b], A. Pompili[a,b], G. Pugliese[a,c], R. Radogna[a], A. Ranieri[a], G. Selvaggi[a,b], L. Silvestris[a], R. Venditti[a], P. Verwilligen[a]

INFN Sezione di Bologna[a], Università di Bologna[b], Bologna, Italy

G. Abbiendi[a], C. Battilana[a,b], D. Bonacorsi[a,b], L. Borgonovi[a,b], S. Braibant-Giacomelli[a,b], R. Campanini[a,b], P. Capiluppi[a,b], A. Castro[a,b], F. R. Cavallo[a], C. Ciocca[a], G. Codispoti[a,b], M. Cuffiani[a,b], G. M. Dallavalle[a], F. Fabbri[a], A. Fanfani[a,b], E. Fontanesi, P. Giacomelli[a], C. Grandi[a], L. Guiducci[a,b], F. Iemmi[a,b], S. Lo Meo[a,29], S. Marcellini[a], G. Masetti[a], F. L. Navarria[a,b], A. Perrotta[a], F. Primavera[a,b], A. M. Rossi[a,b], T. Rovelli[a,b], G. P. Siroli[a,b], N. Tosi[a]

INFN Sezione di Catania[a], Università di Catania[b], Catania, Italy

S. Albergo[a,b,30], S. Costa[a,b], A. Di Mattia[a], R. Potenza[a,b], A. Tricomi[a,b,30], C. Tuve[a,b]

INFN Sezione di Firenze[a], Università di Firenze[b], Firenze, Italy

G. Barbagli[a], R. Ceccarelli, K. Chatterjee[a,b], V. Ciulli[a,b], C. Civinini[a], R. D'Alessandro[a,b], E. Focardi[a,b], G. Latino, P. Lenzi[a,b], M. Meschini[a], S. Paoletti[a], G. Sguazzoni[a], D. Strom[a], L. Viliani[a]

INFN Laboratori Nazionali di Frascati, Frascati, Italy

L. Benussi, S. Bianco, D. Piccolo

INFN Sezione di Genova[a], Università di Genova[b], Genoa, Italy

M. Bozzo[a,b], F. Ferro[a], R. Mulargia[a,b], E. Robutti[a], S. Tosi[a,b]

INFN Sezione di Milano-Bicocca^a, Università di Milano-Bicocca^b, Milan, Italy
A. Benaglia^a, A. Beschi^{a,b}, F. Brivio^{a,b}, V. Ciriolo^{a,b,16}, S. Di Guida^{a,b,16}, M. E. Dinardo^{a,b}, P. Dini^a, S. Fiorendi^{a,b},
S. Gennai^a, A. Ghezzi^{a,b}, P. Govoni^{a,b}, L. Guzzi^{a,b}, M. Malberti^a, S. Malvezzi^a, D. Menasce^a, F. Monti^{a,b}, L. Moroni^a,
G. Ortona^{a,b}, M. Paganoni^{a,b}, D. Pedrini^a, S. Ragazzi^{a,b}, T. Tabarelli de Fatis^{a,b}, D. Zuolo^{a,b}

INFN Sezione di Napoli^a, Università di Napoli 'Federico II' ^{b}, Napoli, Italy, Università della Basilicata^c, Potenza, Italy, Università G. Marconi^d, Rome, Italy
S. Buontempo^a, N. Cavallo^{a,c}, A. De Iorio^{a,b}, A. Di Crescenzo^{a,b}, F. Fabozzi^{a,c}, F. Fienga^a, G. Galati^a, A. O. M. Iorio^{a,b},
L. Lista^{a,b}, S. Meola^{a,d,16}, P. Paolucci^{a,16}, B. Rossi^a, C. Sciacca^{a,b}, E. Voevodina^{a,b}

INFN Sezione di Padova^a, Università di Padova^b, Padua, Italy, Università di Trento^c, Trento, Italy
P. Azzi^a, N. Bacchetta^a, D. D.Bisello^{a,b}, A. Boletti^{a,b}, A. Bragagnolo, R. Carlin^{a,b}, P. Checchia^a, P. De Castro Manzano^a,
T. Dorigo^a, U. Dosselli^a, F. Gasparini^{a,b}, U. Gasparini^{a,b}, A. Gozzelino^a, S. Y. Hoh, P. Lujan, M. Margoni^{a,b},
A. T. Meneguzzo^{a,b}, J. Pazzini^{a,b}, M. Presilla^b, P. Ronchese^{a,b}, R. Rossin^{a,b}, F. Simonetto^{a,b}, A. Tiko, M. Tosi^{a,b},
M. Zanetti^{a,b}, P. Zotto^{a,b}, G. Zumerle^{a,b}

INFN Sezione di Pavia^a, Università di Pavia^b, Pavia, Italy
A. Braghieri^a, P. Montagna^{a,b}, S. P. Ratti^{a,b}, V. Re^a, M. Ressegotti^{a,b}, C. Riccardi^{a,b}, P. Salvini^a, I. Vai^{a,b}, P. Vitulo^{a,b}

INFN Sezione di Perugia^a, Università di Perugia^b, Perugia, Italy
M. Biasini^{a,b}, G. M. Bilei^a, C. Cecchi^{a,b}, D. Ciangottini^{a,b}, L. Fanò^{a,b}, P. Lariccia^{a,b}, R. Leonardi^{a,b}, E. Manoni^a,
G. Mantovani^{a,b}, V. Mariani^{a,b}, M. Menichelli^a, A. Rossi^{a,b}, A. Santocchia^{a,b}, D. Spiga^a

INFN Sezione di Pisa^a, Università di Pisa^b, Scuola Normale Superiore di Pisa^c, Pisa, Italy
K. Androsov^a, P. Azzurri^a, G. Bagliesi^a, V. Bertacchi^{a,c}, L. Bianchini^a, T. Boccali^a, R. Castaldi^a, M. A. Ciocci^{a,b},
R. Dell'Orso^a, G. Fedi^a, L. Giannini^{a,c}, A. Giassi^a, M. T. Grippo^a, F. Ligabue^{a,c}, E. Manca^{a,c}, G. Mandorli^{a,c},
A. Messineo^{a,b}, F. Palla^a, A. Rizzi^{a,b}, G. Rolandi^{31}, S. Roy Chowdhury, A. Scribano^a, P. Spagnolo^a, R. Tenchini^a,
G. Tonelli^{a,b}, N. Turini, A. Venturi^a, P. G. Verdini^a

INFN Sezione di Roma^a, Sapienza Università di Roma^b, Rome, Italy
F. Cavallari^a, M. Cipriani^{a,b}, D. Del Re^{a,b}, E. Di Marco^{a,b}, M. Diemoz^a, E. Longo^{a,b}, B. Marzocchi^{a,b}, P. Meridiani^a,
G. Organtini^{a,b}, F. Pandolfi^a, R. Paramatti^{a,b}, C. Quaranta^{a,b}, S. Rahatlou^{a,b}, C. Rovelli^a, F. Santanastasio^{a,b}, L. Soffi^{a,b}

INFN Sezione di Torino^a, Università di Torino^b, Torino, Italy, Università del Piemonte Orientale^c, Novara, Italy
N. Amapane^{a,b}, R. Arcidiacono^{a,c}, S. Argiro^{a,b}, M. Arneodo^{a,c}, N. Bartosik^a, R. Bellan^{a,b}, C. Biino^a, A. Cappati^{a,b},
N. Cartiglia^a, S. Cometti^a, M. Costa^{a,b}, R. Covarelli^{a,b}, N. Demaria^a, B. Kiani^{a,b}, C. Mariotti^a, S. Maselli^a,
E. Migliore^{a,b}, V. Monaco^{a,b}, E. Monteil^{a,b}, M. Monteno^a, M. M. Obertino^{a,b}, L. Pacher^{a,b}, N. Pastrone^a, M. Pelliccioni^a,
G. L. Pinna Angioni^{a,b}, A. Romero^{a,b}, M. Ruspa^{a,c}, R. Sacchi^{a,c}, R. Salvatico^{a,b}, V. Sola^a, A. Solano^{a,b}, D. Soldi^{a,b},
A. Staiano^a

INFN Sezione di Trieste^a, Università di Trieste^b, Trieste, Italy
S. Belforte^a, V. Candelise^{a,b}, M. Casarsa^a, F. Cossutti^a, A. Da Rold^{a,b}, G. Della Ricca^{a,b}, F. Vazzoler^{a,b}, A. Zanetti^a

Kyungpook National University, Daegu, Korea
B. Kim, D. H. Kim, G. N. Kim, M. S. Kim, J. Lee, S. W. Lee, C. S. Moon, Y. D. Oh, S. I. Pak, S. Sekmen, D. C. Son,
Y. C. Yang

Chonnam National University, Institute for Universe and Elementary Particles, Kwangju, Korea
H. Kim, D. H. Moon, G. Oh

Hanyang University, Seoul, Korea
B. Francois, T. J. Kim, J. Park

Korea University, Seoul, Korea
S. Cho, S. Choi, Y. Go, D. Gyun, S. Ha, B. Hong, K. Lee, K. S. Lee, J. Lim, J. Park, S. K. Park, Y. Roh

Department of Physics, Kyung Hee University, Seoul, Korea
J. Goh

Sejong University, Seoul, Korea
H. S. Kim

Seoul National University, Seoul, Korea
J. Almond, J. H. Bhyun, J. Choi, S. Jeon, J. Kim, J. S. Kim, H. Lee, K. Lee, S. Lee, K. Nam, M. Oh, S. B. Oh,
B. C. Radburn-Smith, U. K. Yang, H. D. Yoo, I. Yoon, G. B. Yu

University of Seoul, Seoul, Korea
D. Jeon, H. Kim, J. H. Kim, J. S. H. Lee, I. C. Park, I. Watson

Sungkyunkwan University, Suwon, Korea
Y. Choi, C. Hwang, Y. Jeong, J. Lee, Y. Lee, I. Yu

Riga Technical University, Riga, Latvia
V. Veckalns[32]

Vilnius University, Vilnius, Lithuania
V. Dudenas, A. Juodagalvis, G. Tamulaitis, J. Vaitkus

National Centre for Particle Physics, Universiti Malaya, Kuala Lumpur, Malaysia
Z. A. Ibrahim, F. Mohamad Idris[33], W. A. T. Wan Abdullah, M. N. Yusli, Z. Zolkapli

Universidad de Sonora (UNISON), Hermosillo, Mexico
J. F. Benitez, A. Castaneda Hernandez, J. A. Murillo Quijada, L. Valencia Palomo

Centro de Investigacion y de Estudios Avanzados del IPN, Mexico City, Mexico
H. Castilla-Valdez, E. De La Cruz-Burelo, I. Heredia-De La Cruz[34], R. Lopez-Fernandez, A. Sanchez-Hernandez

Universidad Iberoamericana, Mexico City, Mexico
S. Carrillo Moreno, C. Oropeza Barrera, M. Ramirez-Garcia, F. Vazquez Valencia

Benemerita Universidad Autonoma de Puebla, Puebla, Mexico
J. Eysermans, I. Pedraza, H. A. Salazar Ibarguen, C. Uribe Estrada

Universidad Autónoma de San Luis Potosí, San Luis Potosí, Mexico
A. Morelos Pineda

University of Montenegro, Podgorica, Montenegro
N. Raicevic

University of Auckland, Auckland, New Zealand
D. Krofcheck

University of Canterbury, Christchurch, New Zealand
S. Bheesette, P. H. Butler

National Centre for Physics, Quaid-I-Azam University, Islamabad, Pakistan
A. Ahmad, M. Ahmad, Q. Hassan, H. R. Hoorani, W. A. Khan, M. A. Shah, M. Shoaib, M. Waqas

AGH University of Science and Technology Faculty of Computer Science, Electronics and Telecommunications, Kraków, Poland
V. Avati, L. Grzanka, M. Malawski

National Centre for Nuclear Research, Swierk, Poland
H. Bialkowska, M. Bluj, B. Boimska, M. Górski, M. Kazana, M. Szleper, P. Zalewski

Institute of Experimental Physics, Faculty of Physics, University of Warsaw, Warsaw, Poland
K. Bunkowski, A. Byszuk[35], K. Doroba, A. Kalinowski, M. Konecki, J. Krolikowski, M. Misiura, M. Olszewski,
A. Pyskir, M. Walczak

Laboratório de Instrumentação e Física Experimental de Partículas, Lisbon, Portugal
M. Araujo, P. Bargassa, D. Bastos, A. Di Francesco, P. Faccioli, B. Galinhas, M. Gallinaro, J. Hollar, N. Leonardo,
J. Seixas, K. Shchelina, G. Strong, O. Toldaiev, J. Varela

Joint Institute for Nuclear Research, Dubna, Russia
P. Bunin, I. Golutvin, I. Gorbunov, A. Kamenev, V. Karjavine, A. Lanev, A. Malakhov, V. Matveev[36,37], P. Moisenz,
V. Palichik, V. Perelygin, M. Savina, S. Shmatov, S. Shulha, A. Zarubin

Petersburg Nuclear Physics Institute, Gatchina (St. Petersburg), Russia
L. Chtchipounov, V. Golovtsov, Y. Ivanov, V. Kim[38], E. Kuznetsova[39], P. Levchenko, V. Murzin, V. Oreshkin, I. Smirnov,
D. Sosnov, V. Sulimov, L. Uvarov, A. Vorobyev

Institute for Nuclear Research, Moscow, Russia
Yu. Andreev, A. Dermenev, S. Gninenko, N. Golubev, A. Karneyeu, M. Kirsanov, N. Krasnikov, A. Pashenkov, D. Tlisov,
A. Toropin

**Institute for Theoretical and Experimental Physics named by A.I. Alikhanov of NRC 'Kurchatov Institute', Moscow,
Russia**
V. Epshteyn, V. Gavrilov, N. Lychkovskaya, A. Nikitenko[40], V. Popov, I. Pozdnyakov, G. Safronov, A. Spiridonov,
A. Stepennov, M. Toms, E. Vlasov, A. Zhokin

Moscow Institute of Physics and Technology, Moscow, Russia
T. Aushev

National Research Nuclear University 'Moscow Engineering Physics Institute' (MEPhI), Moscow, Russia
M. Chadeeva[41], P. Parygin, D. Philippov, E. Popova, V. Rusinov

P.N. Lebedev Physical Institute, Moscow, Russia
V. Andreev, M. Azarkin, I. Dremin, M. Kirakosyan, A. Terkulov

Skobeltsyn Institute of Nuclear Physics, Lomonosov Moscow State University, Moscow, Russia
A. Belyaev, E. Boos, V. Bunichev, M. Dubinin[42], L. Dudko, A. Ershov, A. Gribushin, V. Klyukhin, O. Kodolova,
I. Lokhtin, S. Obraztsov, M. Perfilov, V. Savrin

Novosibirsk State University (NSU), Novosibirsk, Russia
A. Barnyakov[43], V. Blinov[43], T. Dimova[43], L. Kardapoltsev[43], Y. Skovpen[43]

Institute for High Energy Physics of National Research Centre 'Kurchatov Institute', Protvino, Russia
I. Azhgirey, I. Bayshev, S. Bitioukov, V. Kachanov, D. Konstantinov, P. Mandrik, V. Petrov, R. Ryutin, S. Slabospitskii,
A. Sobol, S. Troshin, N. Tyurin, A. Uzunian, A. Volkov

National Research Tomsk Polytechnic University, Tomsk, Russia
A. Babaev, A. Iuzhakov, V. Okhotnikov

Tomsk State University, Tomsk, Russia
V. Borchsh, V. Ivanchenko, E. Tcherniaev

University of Belgrade: Faculty of Physics and VINCA Institute of Nuclear Sciences, Belgrade, Serbia
P. Adzic[44], P. Cirkovic, D. Devetak, M. Dordevic, P. Milenovic, J. Milosevic, M. Stojanovic

Centro de Investigaciones Energéticas Medioambientales y Tecnológicas (CIEMAT), Madrid, Spain
M. Aguilar-Benitez, J. Alcaraz Maestre, A. Álvarez Fernández, I. Bachiller, M. Barrio Luna, J. A. Brochero Cifuentes,
C. A. Carrillo Montoya, M. Cepeda, M. Cerrada, N. Colino, B. De La Cruz, A. Delgado Peris, C. Fernandez Bedoya,
J. P. Fernández Ramos, J. Flix, M. C. Fouz, O. Gonzalez Lopez, S. Goy Lopez, J. M. Hernandez, M. I. Josa, D. Moran,
Á. Navarro Tobar, A. Pérez-Calero Yzquierdo, J. Puerta Pelayo, I. Redondo, L. Romero, S. Sánchez Navas, M. S. Soares,
A. Triossi, C. Willmott

Universidad Autónoma de Madrid, Madrid, Spain
C. Albajar, J. F. de Trocóniz

**Universidad de Oviedo, Instituto Universitario de Ciencias y Tecnologías Espaciales de Asturias (ICTEA), Oviedo,
Spain**
B. Alvarez Gonzalez, J. Cuevas, C. Erice, J. Fernandez Menendez, S. Folgueras, I. Gonzalez Caballero,
J. R. González Fernández, E. Palencia Cortezon, V. Rodríguez Bouza, S. Sanchez Cruz

Instituto de Física de Cantabria (IFCA), CSIC-Universidad de Cantabria, Santander, Spain
I. J. Cabrillo, A. Calderon, B. Chazin Quero, J. Duarte Campderros, M. Fernandez, P. J. Fernández Manteca, A. García Alonso, G. Gomez, C. Martinez Rivero, P. Martinez Ruiz del Arbol, F. Matorras, J. Piedra Gomez, C. Prieels, T. Rodrigo, A. Ruiz-Jimeno, L. Russo[45], L. Scodellaro, N. Trevisani, I. Vila, J. M. Vizan Garcia

University of Colombo, Colombo, Sri Lanka
K. Malagalage

Department of Physics, University of Ruhuna, Matara, Sri Lanka
W. G. D. Dharmaratna, N. Wickramage

CERN, European Organization for Nuclear Research, Geneva, Switzerland
D. Abbaneo, B. Akgun, E. Auffray, G. Auzinger, J. Baechler, P. Baillon, A. H. Ball, D. Barney, J. Bendavid, M. Bianco, A. Bocci, E. Bossini, C. Botta, E. Brondolin, T. Camporesi, A. Caratelli, G. Cerminara, E. Chapon, G. Cucciati, D. d'Enterria, A. Dabrowski, N. Daci, V. Daponte, A. David, O. Davignon, A. De Roeck, N. Deelen, M. Deile, M. Dobson, M. Dünser, N. Dupont, A. Elliott-Peisert, F. Fallavollita[46], D. Fasanella, G. Franzoni, J. Fulcher, W. Funk, S. Giani, D. Gigi, A. Gilbert, K. Gill, F. Glege, M. Gruchala, M. Guilbaud, D. Gulhan, J. Hegeman, C. Heidegger, Y. Iiyama, V. Innocente, P. Janot, O. Karacheban[19], J. Kaspar, J. Kieseler, M. Krammer[1], C. Lange, P. Lecoq, C. Lourenço, L. Malgeri, M. Mannelli, A. Massironi, F. Meijers, J. A. Merlin, S. Mersi, E. Meschi, F. Moortgat, M. Mulders, J. Ngadiuba, S. Nourbakhsh, S. Orfanelli, L. Orsini, F. Pantaleo[16], L. Pape, E. Perez, M. Peruzzi, A. Petrilli, G. Petrucciani, A. Pfeiffer, M. Pierini, F. M. Pitters, D. Rabady, A. Racz, M. Rovere, H. Sakulin, C. Schäfer, C. Schwick, M. Selvaggi, A. Sharma, P. Silva, W. Snoeys, P. Sphicas[47], J. Steggemann, V. R. Tavolaro, D. Treille, A. Tsirou, A. Vartak, M. Verzetti, W. D. Zeuner

Paul Scherrer Institut, Villigen, Switzerland
L. Caminada[48], K. Deiters, W. Erdmann, R. Horisberger, Q. Ingram, H. C. Kaestli, D. Kotlinski, U. Langenegger, T. Rohe, S. A. Wiederkehr

ETH Zurich-Institute for Particle Physics and Astrophysics (IPA), Zürich, Switzerland
M. Backhaus, P. Berger, N. Chernyavskaya, G. Dissertori, M. Dittmar, M. Donegà, C. Dorfer, T. A. Gómez Espinosa, C. Grab, D. Hits, T. Klijnsma, W. Lustermann, R. A. Manzoni, M. Marionneau, M. T. Meinhard, F. Micheli, P. Musella, F. Nessi-Tedaldi, F. Pauss, G. Perrin, L. Perrozzi, S. Pigazzini, M. Reichmann, C. Reissel, T. Reitenspiess, D. Ruini, D. A. Sanz Becerra, M. Schönenberger, L. Shchutska, M. L. Vesterbacka Olsson, R. Wallny, D. H. Zhu

Universität Zürich, Zürich, Switzerland
T. K. Aarrestad, C. Amsler[49], D. Brzhechko, M. F. Canelli, A. De Cosa, R. Del Burgo, S. Donato, B. Kilminster, S. Leontsinis, V. M. Mikuni, I. Neutelings, G. Rauco, P. Robmann, D. Salerno, K. Schweiger, C. Seitz, Y. Takahashi, S. Wertz, A. Zucchetta

National Central University, Chung-Li, Taiwan
T. H. Doan, C. M. Kuo, W. Lin, A. Roy, S. S. Yu

National Taiwan University (NTU), Taipei, Taiwan
P. Chang, Y. Chao, K. F. Chen, P. H. Chen, W.-S. Hou, Y. y. Li, R.-S. Lu, E. Paganis, A. Psallidas, A. Steen

Chulalongkorn University, Faculty of Science, Department of Physics, Bangkok, Thailand
B. Asavapibhop, C. Asawatangtrakuldee, N. Srimanobhas, N. Suwonjandee

Çukurova University, Physics Department, Science and Art Faculty, Adana, Turkey
A. Bat, F. Boran, S. Cerci[50], S. Damarseckin[51], Z. S. Demiroglu, F. Dolek, C. Dozen, I. Dumanoglu, G. Gokbulut, EmineGurpinar Guler[52], Y. Guler, I. Hos[53], C. Isik, E. E. Kangal[54], O. Kara, A. Kayis Topaksu, U. Kiminsu, M. Oglakci, G. Onengut, K. Ozdemir[55], S. Ozturk[56], A. E. Simsek, D. Sunar Cerci[50], U. G. Tok, S. Turkcapar, I. S. Zorbakir, C. Zorbilmez

Middle East Technical University, Physics Department, Ankara, Turkey
B. Isildak[57], G. Karapinar[58], M. Yalvac

Bogazici University, Istanbul, Turkey
I. O. Atakisi, E. Gülmez, M. Kaya[59], O. Kaya[60], B. Kaynak, Ö. Özçelik, S. Tekten, E. A. Yetkin[61]

Istanbul Technical University, Istanbul, Turkey
A. Cakir, K. Cankocak, Y. Komurcu, S. Sen[62]

Istanbul University, Istanbul, Turkey
S. Ozkorucuklu

Institute for Scintillation Materials of National Academy of Science of Ukraine, Kharkov, Ukraine
B. Grynyov

National Scientific Center, Kharkov Institute of Physics and Technology, Kharkov, Ukraine
L. Levchuk

University of Bristol, Bristol, UK
F. Ball, E. Bhal, S. Bologna, J. J. Brooke, D. Burns, E. Clement, D. Cussans, H. Flacher, J. Goldstein, G. P. Heath,
H. F. Heath, L. Kreczko, S. Paramesvaran, B. Penning, T. Sakuma, S. Seif El Nasr-Storey, D. Smith, V. J. Smith, J. Taylor,
A. Titterton

Rutherford Appleton Laboratory, Didcot, UK
K. W. Bell, A. Belyaev[63], C. Brew, R. M. Brown, D. Cieri, D. J. A. Cockerill, J. A. Coughlan, K. Harder, S. Harper,
J. Linacre, K. Manolopoulos, D. M. Newbold, E. Olaiya, D. Petyt, T. Reis, T. Schuh, C. H. Shepherd-Themistocleous,
A. Thea, I. R. Tomalin, T. Williams, W. J. Womersley

Imperial College, London, UK
R. Bainbridge, P. Bloch, J. Borg, S. Breeze, O. Buchmuller, A. Bundock, GurpreetSingh CHAHAL[64], D. Colling,
P. Dauncey, G. Davies, M. Della Negra, R. Di Maria, P. Everaerts, G. Hall, G. Iles, T. James, M. Komm, C. Laner,
L. Lyons, A.-M. Magnan, S. Malik, A. Martelli, V. Milosevic, J. Nash[65], V. Palladino, M. Pesaresi, D. M. Raymond,
A. Richards, A. Rose, E. Scott, C. Seez, A. Shtipliyski, M. Stoye, T. Strebler, S. Summers, A. Tapper, K. Uchida,
T. Virdee[16], N. Wardle, D. Winterbottom, J. Wright, A. G. Zecchinelli, S. C. Zenz

Brunel University, Uxbridge, UK
J. E. Cole, P. R. Hobson, A. Khan, P. Kyberd, C. K. Mackay, A. Morton, I. D. Reid, L. Teodorescu, S. Zahid

Baylor University, Waco, USA
K. Call, J. Dittmann, K. Hatakeyama, C. Madrid, B. McMaster, N. Pastika, C. Smith

Catholic University of America, Washington DC, USA
R. Bartek, A. Dominguez, R. Uniyal

The University of Alabama, Tuscaloosa, USA
A. Buccilli, S. I. Cooper, C. Henderson, P. Rumerio, C. West

Boston University, Boston, USA
D. Arcaro, T. Bose, Z. Demiragli, D. Gastler, S. Girgis, D. Pinna, C. Richardson, J. Rohlf, D. Sperka, I. Suarez, L. Sulak,
D. Zou

Brown University, Providence, USA
G. Benelli, B. Burkle, X. Coubez, D. Cutts, Y. t. Duh, M. Hadley, J. Hakala, U. Heintz, J. M. Hogan[66], K. H. M. Kwok,
E. Laird, G. Landsberg, J. Lee, Z. Mao, M. Narain, S. Sagir[67], R. Syarif, E. Usai, D. Yu

University of California, Davis, Davis, USA
R. Band, C. Brainerd, R. Breedon, M. Calderon De La Barca Sanchez, M. Chertok, J. Conway, R. Conway, P. T. Cox,
R. Erbacher, C. Flores, G. Funk, F. Jensen, W. Ko, O. Kukral, R. Lander, M. Mulhearn, D. Pellett, J. Pilot, M. Shi,
D. Stolp, D. Taylor, K. Tos, M. Tripathi, Z. Wang, F. Zhang

University of California, Los Angeles, USA
M. Bachtis, C. Bravo, R. Cousins, A. Dasgupta, A. Florent, J. Hauser, M. Ignatenko, N. Mccoll, W. A. Nash, S. Regnard,
D. Saltzberg, C. Schnaible, B. Stone, V. Valuev

University of California, Riverside, Riverside, USA

K. Burt, R. Clare, J. W. Gary, S. M. A. Ghiasi Shirazi, G. Hanson, G. Karapostoli, E. Kennedy, O. R. Long, M. Olmedo Negrete, M. I. Paneva, W. Si, L. Wang, H. Wei, S. Wimpenny, B. R. Yates, Y. Zhang

University of California, San Diego, La Jolla, USA

J. G. Branson, P. Chang, S. Cittolin, M. Derdzinski, R. Gerosa, D. Gilbert, B. Hashemi, D. Klein, V. Krutelyov, J. Letts, M. Masciovecchio, S. May, S. Padhi, M. Pieri, V. Sharma, M. Tadel, F. Würthwein, A. Yagil, G. Zevi Della Porta

University of California, Santa Barbara-Department of Physics, Santa Barbara, USA

N. Amin, R. Bhandari, C. Campagnari, M. Citron, V. Dutta, M. Franco Sevilla, L. Gouskos, J. Incandela, B. Marsh, H. Mei, A. Ovcharova, H. Qu, J. Richman, U. Sarica, D. Stuart, S. Wang, J. Yoo

California Institute of Technology, Pasadena, USA

D. Anderson, A. Bornheim, O. Cerri, I. Dutta, J. M. Lawhorn, N. Lu, J. Mao, H. B. Newman, T. Q. Nguyen, J. Pata, M. Spiropulu, J. R. Vlimant, S. Xie, Z. Zhang, R. Y. Zhu

Carnegie Mellon University, Pittsburgh, USA

M. B. Andrews, T. Ferguson, T. Mudholkar, M. Paulini, M. Sun, I. Vorobiev, M. Weinberg

University of Colorado Boulder, Boulder, USA

J. P. Cumalat, W. T. Ford, A. Johnson, E. MacDonald, T. Mulholland, R. Patel, A. Perloff, K. Stenson, K. A. Ulmer, S. R. Wagner

Cornell University, Ithaca, USA

J. Alexander, J. Chaves, Y. Cheng, J. Chu, A. Datta, A. Frankenthal, K. Mcdermott, N. Mirman, J. R. Patterson, D. Quach, A. Rinkevicius[68], A. Ryd, S. M. Tan, Z. Tao, J. Thom, P. Wittich, M. Zientek

Fermi National Accelerator Laboratory, Batavia, USA

S. Abdullin, M. Albrow, M. Alyari, G. Apollinari, A. Apresyan, A. Apyan, S. Banerjee, L. A. T. Bauerdick, A. Beretvas, J. Berryhill, P. C. Bhat, K. Burkett, J. N. Butler, A. Canepa, G. B. Cerati, H. W. K. Cheung, F. Chlebana, M. Cremonesi, J. Duarte, V. D. Elvira, J. Freeman, Z. Gecse, E. Gottschalk, L. Gray, D. Green, S. Grünendahl, O. Gutsche, AllisonReinsvold Hall, J. Hanlon, R. M. Harris, S. Hasegawa, R. Heller, J. Hirschauer, B. Jayatilaka, S. Jindariani, M. Johnson, U. Joshi, B. Klima, M. J. Kortelainen, B. Kreis, S. Lammel, J. Lewis, D. Lincoln, R. Lipton, M. Liu, T. Liu, J. Lykken, K. Maeshima, J. M. Marraffino, D. Mason, P. McBride, P. Merkel, S. Mrenna, S. Nahn, V. O'Dell, V. Papadimitriou, K. Pedro, C. Pena, G. Rakness, F. Ravera, L. Ristori, B. Schneider, E. Sexton-Kennedy, N. Smith, A. Soha, W. J. Spalding, L. Spiegel, S. Stoynev, J. Strait, N. Strobbe, L. Taylor, S. Tkaczyk, N. V. Tran, L. Uplegger, E. W. Vaandering, C. Vernieri, M. Verzocchi, R. Vidal, M. Wang, H. A. Weber

University of Florida, Gainesville, USA

D. Acosta, P. Avery, P. Bortignon, D. Bourilkov, A. Brinkerhoff, L. Cadamuro, A. Carnes, V. Cherepanov, D. Curry, F. Errico, R. D. Field, S. V. Gleyzer, B. M. Joshi, M. Kim, J. Konigsberg, A. Korytov, K. H. Lo, P. Ma, K. Matchev, N. Menendez, G. Mitselmakher, D. Rosenzweig, K. Shi, J. Wang, S. Wang, X. Zuo

Florida International University, Miami, USA

Y. R. Joshi

Florida State University, Tallahassee, USA

T. Adams, A. Askew, S. Hagopian, V. Hagopian, K. F. Johnson, R. Khurana, T. Kolberg, G. Martinez, T. Perry, H. Prosper, C. Schiber, R. Yohay, J. Zhang

Florida Institute of Technology, Melbourne, USA

M. M. Baarmand, V. Bhopatkar, M. Hohlmann, D. Noonan, M. Rahmani, M. Saunders, F. Yumiceva

University of Illinois at Chicago (UIC), Chicago, USA

M. R. Adams, L. Apanasevich, D. Berry, R. R. Betts, R. Cavanaugh, X. Chen, S. Dittmer, O. Evdokimov, C. E. Gerber, D. A. Hangal, D. J. Hofman, K. Jung, C. Mills, T. Roy, M. B. Tonjes, N. Varelas, H. Wang, X. Wang, Z. Wu

The University of Iowa, Iowa City, USA

M. Alhusseini, B. Bilki[52], W. Clarida, K. Dilsiz[69], S. Durgut, R. P. Gandrajula, M. Haytmyradov, V. Khristenko,

O. K. Köseyan, J.-P. Merlo, A. Mestvirishvili[70], A. Moeller, J. Nachtman, H. Ogul[71], Y. Onel, F. Ozok[72], A. Penzo, C. Snyder, E. Tiras, J. Wetzel

Johns Hopkins University, Baltimore, USA
B. Blumenfeld, A. Cocoros, N. Eminizer, D. Fehling, L. Feng, A. V. Gritsan, W. T. Hung, P. Maksimovic, J. Roskes, M. Swartz, M. Xiao

The University of Kansas, Lawrence, USA
C. Baldenegro Barrera, P. Baringer, A. Bean, S. Boren, J. Bowen, A. Bylinkin, T. Isidori, S. Khalil, J. King, G. Krintiras, A. Kropivnitskaya, C. Lindsey, D. Majumder, W. Mcbrayer, N. Minafra, M. Murray, C. Rogan, C. Royon, S. Sanders, E. Schmitz, J. D. Tapia Takaki, Q. Wang, J. Williams, G. Wilson

Kansas State University, Manhattan, USA
S. Duric, A. Ivanov, K. Kaadze, D. Kim, Y. Maravin, D. R. Mendis, T. Mitchell, A. Modak, A. Mohammadi

Lawrence Livermore National Laboratory, Livermore, USA
F. Rebassoo, D. Wright

University of Maryland, College Park, USA
A. Baden, O. Baron, A. Belloni, S. C. Eno, Y. Feng, N. J. Hadley, S. Jabeen, G. Y. Jeng, R. G. Kellogg, J. Kunkle, A. C. Mignerey, S. Nabili, F. Ricci-Tam, M. Seidel, Y. H. Shin, A. Skuja, S. C. Tonwar, K. Wong

Massachusetts Institute of Technology, Cambridge, USA
D. Abercrombie, B. Allen, A. Baty, R. Bi, S. Brandt, W. Busza, I. A. Cali, M. D'Alfonso, G. Gomez Ceballos, M. Goncharov, P. Harris, D. Hsu, M. Hu, M. Klute, D. Kovalskyi, Y.-J. Lee, P. D. Luckey, B. Maier, A. C. Marini, C. Mcginn, C. Mironov, S. Narayanan, X. Niu, C. Paus, D. Rankin, C. Roland, G. Roland, Z. Shi, G. S. F. Stephans, K. Sumorok, K. Tatar, D. Velicanu, J. Wang, T. W. Wang, B. Wyslouch

University of Minnesota, Minneapolis, USA
A. C. Benvenuti[†], R. M. Chatterjee, A. Evans, S. Guts, P. Hansen, J. Hiltbrand, Sh. Jain, S. Kalafut, Y. Kubota, Z. Lesko, J. Mans, R. Rusack, M. A. Wadud

University of Mississippi, Oxford, USA
J. G. Acosta, S. Oliveros

University of Nebraska-Lincoln, Lincoln, USA
K. Bloom, D. R. Claes, C. Fangmeier, L. Finco, F. Golf, R. Gonzalez Suarez, R. Kamalieddin, I. Kravchenko, J. E. Siado, G. R. Snow, B. Stieger

State University of New York at Buffalo, Buffalo, USA
G. Agarwal, C. Harrington, I. Iashvili, A. Kharchilava, C. Mclean, D. Nguyen, A. Parker, J. Pekkanen, S. Rappoccio, B. Roozbahani

Northeastern University, Boston, USA
G. Alverson, E. Barberis, C. Freer, Y. Haddad, A. Hortiangtham, G. Madigan, D. M. Morse, T. Orimoto, L. Skinnari, A. Tishelman-Charny, T. Wamorkar, B. Wang, A. Wisecarver, D. Wood

Northwestern University, Evanston, USA
S. Bhattacharya, J. Bueghly, T. Gunter, K. A. Hahn, N. Odell, M. H. Schmitt, K. Sung, M. Trovato, M. Velasco

University of Notre Dame, Notre Dame, USA
R. Bucci, N. Dev, R. Goldouzian, M. Hildreth, K. Hurtado Anampa, C. Jessop, D. J. Karmgard, K. Lannon, W. Li, N. Loukas, N. Marinelli, I. Mcalister, F. Meng, C. Mueller, Y. Musienko[36], M. Planer, R. Ruchti, P. Siddireddy, G. Smith, S. Taroni, M. Wayne, A. Wightman, M. Wolf, A. Woodard

The Ohio State University, Columbus, USA
J. Alimena, B. Bylsma, L. S. Durkin, S. Flowers, B. Francis, C. Hill, W. Ji, A. Lefeld, T. Y. Ling, B. L. Winer

Princeton University, Princeton, USA
S. Cooperstein, G. Dezoort, P. Elmer, J. Hardenbrook, N. Haubrich, S. Higginbotham, A. Kalogeropoulos, S. Kwan,

D. Lange, M. T. Lucchini, J. Luo, D. Marlow, K. Mei, I. Ojalvo, J. Olsen, C. Palmer, P. Piroué, J. Salfeld-Nebgen, D. Stickland, C. Tully, Z. Wang

University of Puerto Rico, Mayaguez, USA

S. Malik, S. Norberg

Purdue University, West Lafayette, USA

A. Barker, V. E. Barnes, S. Das, L. Gutay, M. Jones, A. W. Jung, A. Khatiwada, B. Mahakud, D. H. Miller, G. Negro, N. Neumeister, C. C. Peng, S. Piperov, H. Qiu, J. F. Schulte, J. Sun, F. Wang, R. Xiao, W. Xie

Purdue University Northwest, Hammond, USA

T. Cheng, J. Dolen, N. Parashar

Rice University, Houston, USA

K. M. Ecklund, S. Freed, F. J. M. Geurts, M. Kilpatrick, Arun Kumar, W. Li, B. P. Padley, R. Redjimi, J. Roberts, J. Rorie, W. Shi, A. G. Stahl Leiton, Z. Tu, A. Zhang

University of Rochester, Rochester, USA

A. Bodek, P. de Barbaro, R. Demina, J. L. Dulemba, C. Fallon, T. Ferbel, M. Galanti, A. Garcia-Bellido, J. Han, O. Hindrichs, A. Khukhunaishvili, E. Ranken, P. Tan, R. Taus

Rutgers, The State University of New Jersey, Piscataway, USA

B. Chiarito, J. P. Chou, A. Gandrakota, Y. Gershtein, E. Halkiadakis, A. Hart, M. Heindl, E. Hughes, S. Kaplan, S. Kyriacou, I. Laflotte, A. Lath, R. Montalvo, K. Nash, M. Osherson, H. Saka, S. Salur, S. Schnetzer, D. Sheffield, S. Somalwar, R. Stone, S. Thomas, P. Thomassen

University of Tennessee, Knoxville, USA

H. Acharya, A. G. Delannoy, J. Heideman, G. Riley, S. Spanier

Texas A & M University, College Station, USA

O. Bouhali[73], A. Celik, M. Dalchenko, M. De Mattia, A. Delgado, S. Dildick, R. Eusebi, J. Gilmore, T. Huang, T. Kamon[74], S. Luo, D. Marley, R. Mueller, D. Overton, L. Perniè, D. Rathjens, A. Safonov

Texas Tech University, Lubbock, USA

N. Akchurin, J. Damgov, F. De Guio, S. Kunori, K. Lamichhane, S. W. Lee, T. Mengke, S. Muthumuni, T. Peltola, S. Undleeb, I. Volobouev, Z. Wang, A. Whitbeck

Vanderbilt University, Nashville, USA

S. Greene, A. Gurrola, R. Janjam, W. Johns, C. Maguire, A. Melo, H. Ni, K. Padeken, F. Romeo, P. Sheldon, S. Tuo, J. Velkovska, M. Verweij

University of Virginia, Charlottesville, USA

M. W. Arenton, P. Barria, B. Cox, G. Cummings, R. Hirosky, M. Joyce, A. Ledovskoy, C. Neu, B. Tannenwald, Y. Wang, E. Wolfe, F. Xia

Wayne State University, Detroit, USA

R. Harr, P. E. Karchin, N. Poudyal, J. Sturdy, P. Thapa, S. Zaleski

University of Wisconsin-Madison, Madison, WI, USA

J. Buchanan, C. Caillol, D. Carlsmith, S. Dasu, I. De Bruyn, L. Dodd, F. Fiori, C. Galloni, B. Gomber[75], M. Herndon, A. Hervé, U. Hussain, P. Klabbers, A. Lanaro, A. Loeliger, K. Long, R. Loveless, J. Madhusudanan Sreekala, T. Ruggles, A. Savin, V. Sharma, W. H. Smith, D. Teague, S. Trembath-reichert, N. Woods

† **Deceased**

1: Also at Vienna University of Technology, Vienna, Austria
2: Also at IRFU, CEA, Université Paris-Saclay, Gif-sur-Yvette, France
3: Also at Universidade Estadual de Campinas, Campinas, Brazil
4: Also at Federal University of Rio Grande do Sul, Porto Alegre, Brazil
5: Also at UFMS, Nova Andradina, Brazil

6: Also at Universidade Federal de Pelotas, Pelotas, Brazil

7: Also at Université Libre de Bruxelles, Bruxelles, Belgium

8: Also at University of Chinese Academy of Sciences, Beijing, China

9: Also at Institute for Theoretical and Experimental Physics named by A.I. Alikhanov of NRC 'Kurchatov Institute', Moscow, Russia

10: Also at Joint Institute for Nuclear Research, Dubna, Russia

11: Also at Ain Shams University, Cairo, Egypt

12: Also at Zewail City of Science and Technology, Zewail, Egypt

13: Also at Purdue University, West Lafayette, USA

14: Also at Université de Haute Alsace, Mulhouse, France

15: Also at Erzincan Binali Yildirim University,Erzincan,Turkey

16: Also at CERN, European Organization for Nuclear Research, Geneva, Switzerland

17: Also at RWTH Aachen University, III. Physikalisches Institut A, Aachen, Germany

18: Also at University of Hamburg, Hamburg, Germany

19: Also at Brandenburg University of Technology, Cottbus, Germany

20: Also at Institute of Physics, University of Debrecen, Debrecen, Hungary, Debrecen, Hungary

21: Also at Institute of Nuclear Research ATOMKI, Debrecen, Hungary

22: Also at MTA-ELTE Lendület CMS Particle and Nuclear Physics Group, Eötvös Loránd University, Budapest, Hungary, Budapest, Hungary

23: Also at IIT Bhubaneswar, Bhubaneswar, India, Bhubaneswar, India

24: Also at Institute of Physics, Bhubaneswar, India

25: Also at Shoolini University, Solan, India

26: Also at University of Visva-Bharati, Santiniketan, India

27: Also at Isfahan University of Technology, Isfahan, Iran

28: Now at INFN Sezione di Bari^a, Università di Bari^b, Politecnico di Bari^c, Bari, Italy

29: Also at Italian National Agency for New Technologies, Energy and Sustainable Economic Development, Bologna, Italy

30: Also at Centro Siciliano di Fisica Nucleare e di Struttura Della Materia, Catania, Italy

31: Also at Scuola Normale e Sezione dell'INFN, Pisa, Italy

32: Also at Riga Technical University, Riga, Latvia, Riga, Latvia

33: Also at Malaysian Nuclear Agency, MOSTI, Kajang, Malaysia

34: Also at Consejo Nacional de Ciencia y Tecnología, Mexico City, Mexico

35: Also at Warsaw University of Technology, Institute of Electronic Systems, Warsaw, Poland

36: Also at Institute for Nuclear Research, Moscow, Russia

37: Now at National Research Nuclear University 'Moscow Engineering Physics Institute' (MEPhI), Moscow, Russia

38: Also at St. Petersburg State Polytechnical University, St. Petersburg, Russia

39: Also at University of Florida, Gainesville, USA

40: Also at Imperial College, London, UK

41: Also at P.N. Lebedev Physical Institute, Moscow, Russia

42: Also at California Institute of Technology, Pasadena, USA

43: Also at Budker Institute of Nuclear Physics, Novosibirsk, Russia

44: Also at Faculty of Physics, University of Belgrade, Belgrade, Serbia

45: Also at Università degli Studi di Siena, Siena, Italy

46: Also at INFN Sezione di Pavia^a, Università di Pavia^b, Pavia, Italy, Pavia, Italy

47: Also at National and Kapodistrian University of Athens, Athens, Greece

48: Also at Universität Zürich, Zurich, Switzerland

49: Also at Stefan Meyer Institute for Subatomic Physics, Vienna, Austria, Vienna, Austria

50: Also at Adiyaman University, Adiyaman, Turkey

51: Also at Şırnak University, Sirnak, Turkey

52: Also at Beykent University, Istanbul, Turkey, Istanbul, Turkey

53: Also at Istanbul Aydin University, Application and Research Center for Advanced Studies (App. & Res. Cent. for Advanced Studies), Istanbul, Turkey

54: Also at Mersin University, Mersin, Turkey

55: Also at Piri Reis University, Istanbul, Turkey

56: Also at Gaziosmanpasa University, Tokat, Turkey

57: Also at Ozyegin University, Istanbul, Turkey

58: Also at Izmir Institute of Technology, Izmir, Turkey

59: Also at Marmara University, Istanbul, Turkey

60: Also at Kafkas University, Kars, Turkey

61: Also at Istanbul Bilgi University, Istanbul, Turkey

62: Also at Hacettepe University, Ankara, Turkey

63: Also at School of Physics and Astronomy, University of Southampton, Southampton, UK

64: Also at IPPP Durham University, Durham, UK

65: Also at Monash University, Faculty of Science, Clayton, Australia

66: Also at Bethel University, St. Paul, Minneapolis, USA, St. Paul, USA

67: Also at Karamanoğlu Mehmetbey University, Karaman, Turkey

68: Also at Vilnius University, Vilnius, Lithuania

69: Also at Bingol University, Bingol, Turkey

70: Also at Georgian Technical University, Tbilisi, Georgia

71: Also at Sinop University, Sinop, Turkey

72: Also at Mimar Sinan University, Istanbul, Istanbul, Turkey

73: Also at Texas A&M University at Qatar, Doha, Qatar

74: Also at Kyungpook National University, Daegu, Korea, Daegu, Korea

75: Also at University of Hyderabad, Hyderabad, India